TAMPEREEN TEKNILLINEN YLIOPISTO
TAMPERE UNIVERSITY OF TECHNOLOGY
Julkaisu 579 • Publication 579

Antti Lehtinen

Analytical Treatment of Heat Sinks Cooled by Forced Convection

Tampere 2005

Tampereen teknillinen yliopisto. Julkaisu 579
Tampere University of Technology. Publication 579

Antti Lehtinen

Analytical Treatment of Heat Sinks Cooled by Forced Convection

Thesis for the degree of Doctor of Technology to be presented with due permission for public examination and criticism in Konetalo Building, Auditorium K1703, at Tampere University of Technology, on the 22nd of December 2005, at 12 noon.

Tampereen teknillinen yliopisto - Tampere University of Technology
Tampere 2005

ISBN 952-15-1512-0 (printed)
ISBN 952-15-1531-7 (PDF)
ISSN 1459-2045

Abstract

Understanding heat transfer is vital in numerous applications in the field of power electronics. This thesis introduces some new reliable and efficient calculation methods for plate-fin heat sinks. There may be any number of electronic components attached to the base plate. The components may have arbitrary prescribed heat flux distribution. The state-of-the-art calculation methods found in the literature are based on conduction analysis, while the convective heat transfer is only treated as a boundary condition. This may lead to unphysical solutions. In this thesis, conjugated conduction and convection heat transfer problem is solved in the fins. However, the tedious solution of the Navier-Stokes equations is avoided by applying well-known analytical and experimental results for convective heat transfer. The conjugated heat transfer solution for the fins is used to determine the temperature field of the base plate. Some numerical examples are given to illustrate the fact that the present calculation methods give physically more realistic results than the methods found in the literature. The analysis in this thesis has been carried out assuming steady-state conditions. However, it is pointed out that the methods presented in the thesis can easily be generalised for the transient operation of the electronic components.

Preface

This thesis has been written while I have been working as an assistant at Tampere University of Technology, Institute of Energy and Process Engineering.

I am grateful to Prof. Reijo Karvinen, who has guided me and given valuable advice throughout the work. He has provided me with an excellent environment for scientific research.

I also wish to express my thanks to Prof. M. Michael Yovanovich and Prof. Andris Buikis, who have given excellent comments and remarks concerning my thesis.

Furthermore, I would like to thank ABB Oy and Outokumpu Poricopper Oy for the financial support during the work.

Finally, I also want to thank my family for the support during the work.

Tampere, December 7th 2005,

Antti Lehtinen

Nomenclature

Roman letters:

a	Base plate thickness
A_{ij}	Coefficients in Eq. (3.4)
$\boldsymbol{a_j}$	Vector composed of coefficients A_{ij}, see Eq. (6.12)
b	Fin half-spacing
B_{ij}	Coefficients in Eq. (3.4)
$\boldsymbol{b_j}$	Vector composed of coefficients B_{ij}, see Eq. (6.12)
c_f	Friction factor
C_i	Coefficients in Eq. (4.6)
c_p	Fluid specific heat
D_i	Coefficients in Eq. (4.6)
$\boldsymbol{E_j}$	Matrix in Eq. (6.14)
$E_{j,iI}$	Element of matrix $\boldsymbol{E_j}$ on row i and column I, indexing begins from zero
f	Arbitrary function
f_i	Coefficient or function in Eqs. (A.1) and (A.6)
f_{ij}	Function in Eq. (A.7)
G_n	Graetz solution coefficient
H	Heat sink width in direction normal to fins, see Figs. 1.1 and 1.2
h	Heat transfer coefficient based on fluid inlet temperature
h_m	Heat transfer coefficient based on mixed mean flow temperature
h_{eff}	Effective heat transfer coefficient at top of base plate
i, I	Eigenvalue number in x-direction

j	Eigenvalue number in z-direction
k_a	Fluid thermal conductivity
k_b	Base plate thermal conductivity
k_f	Fin thermal conductivity
L	Heat sink length in flow direction, see Fig. 1.1
l	Fin length in direction normal to base plate, see Figs. 1.1 and 1.2
L^+	Dimensionless fin length in flow direction, see Eq. (2.9)
m	$\sqrt{h/(k_f t)}$, fin parameter
$\dot{m}$	Total mass flow rate through the heat sink
$\boldsymbol{M}$	Square root of matrix $\boldsymbol{M}^2$
$\boldsymbol{M}^2$	Matrix in Eq. (5.9)
${M^2}_{iI}$	Element of matrix $\boldsymbol{M}^2$ on row i and column I, indexing begins from zero
n	Eigenvalue number of Graetz solution
N_f	Number of fins in heat sink
N_i	Number of terms in summation in x-direction
N_j	Number of terms in summation in z-direction
N_{tu}	Number of transfer units, see Eq. (2.20)
Nu_m	$\dfrac{4bh_m}{k_a}$, mean Nusselt number
p	Summation index
Pr	$\dfrac{\rho c_p \nu}{k_a}$, Prandtl number
Q	Total heat transfer rate of the heat sink
q	Convective heat transfer rate from fins, heat flux at bottom of base plate
Q_{ij}	Fourier coefficients of bottom heat flux, see Eq. (3.7)
$\boldsymbol{q_j}$	Vector composed of coefficients Q_{ij}, see Eq. (6.12)
r	$\dfrac{k_f t}{k_b(t+b)}$, dimensionless fin thickness parameter
$\boldsymbol{R}$	Matrix in Eq. (5.19)
R_{iI}	Element of matrix $\boldsymbol{R}$ on row i and column I, indexing begins from zero

R_{fins} Fin-side thermal resistance θ_b/Q

Re $\frac{4Ub}{\nu}$, Reynolds number

T Matrix transpose

t Fin half-thickness

T_∞ Fluid inlet temperature

T_a Fluid temperature

T_b Base plate temperature

T_f Fin temperature

T_m Fluid mixed mean temperature

U Fluid mean velocity

u Velocity in the x-direction

$\boldsymbol{V}$ Matrix composed of eigenvectors of matrix $\boldsymbol{M}$

x Coordinate in the direction of flow, see Fig. 1.1

$\boldsymbol{X}$ Arbitrary matrix

x^+ Dimensionless x-coordinate, see Eq. (2.13)

y Coordinate in the direction normal to base plate, see Figs. 1.1 and 1.2

z Coordinate in the direction normal to fins, see Figs. 1.1 and 1.2

Greek letters:

α_I $I\pi/L$, eigenvalue in x-direction

α_i $i\pi/L$, eigenvalue in x-direction

β_j $j\pi/H$, eigenvalue in z-direction

δ Delta function, see Eq. (A.4)

ϵ Heat transfer effectiveness, see Eq. (2.19)

γ_{ij} $\sqrt{\alpha_i^2 + \beta_j^2}$, separation constant

$\boldsymbol{\Lambda}$ Diagonal matrix composed of eigenvalues of matrix $\boldsymbol{M}$

λ_n Graetz solution eigenvalue

μ_i $\sqrt{m^2 + \alpha_i^2}$, separation constant

ν Fluid kinematic viscosity

ρ	Fluid density
θ_b	Base plate temperature excess $T_b - T_\infty$
$\theta_{b,ij}$	Fourier coefficient functions of θ_b in Eq. (3.2)
θ_f	Fin temperature excess $T_f - T_\infty$
$\boldsymbol{\theta_f}$	Vector-valued function composed of functions $\theta_{f,i}$
$\theta_{f,i}$	Fourier coefficient functions of θ_f in Eq. (4.4)
θ_m	Mixed mean temperature excess $T_m - T_\infty$
ξ	Dummy variable in integrals in x-direction

Contents

Chapter 1

Introduction

1.1 Background and motivation

One of the most difficult challenges in modern power electronics is obtaining sufficient cooling for the components. The operating temperature of the components is an extremely important factor affecting their reliability. The usual cooling arrangement is attaching the components at a heat sink that is cooled by liquid or air. The heat sink typically consists of a base plate and a stack of fins. A commonly used plate-fin arrangement is shown schematically in Figs. 1.1 and 1.2. In addition, as the dissipated heat of the components grows, a fan or a pump is needed to obtain higher rates of heat transfer by forced convection.

The design process of a heat sink for a given set electronic components is a very complicated task involving many contradicting optimisation criteria. The goal is to minimise the following:

- Temperature of the component(s)
- Fluid outflow temperature (for safety reasons)
- Manufacturing costs
- Mass
- Outer dimensions
- Operating costs
- Purchasing and operating costs of a fan or a pump
- Noise

Generating an overall cost function for assessing the goodness of a particular heat sink design is difficult. The cost function is certainly highly nonlinear at least

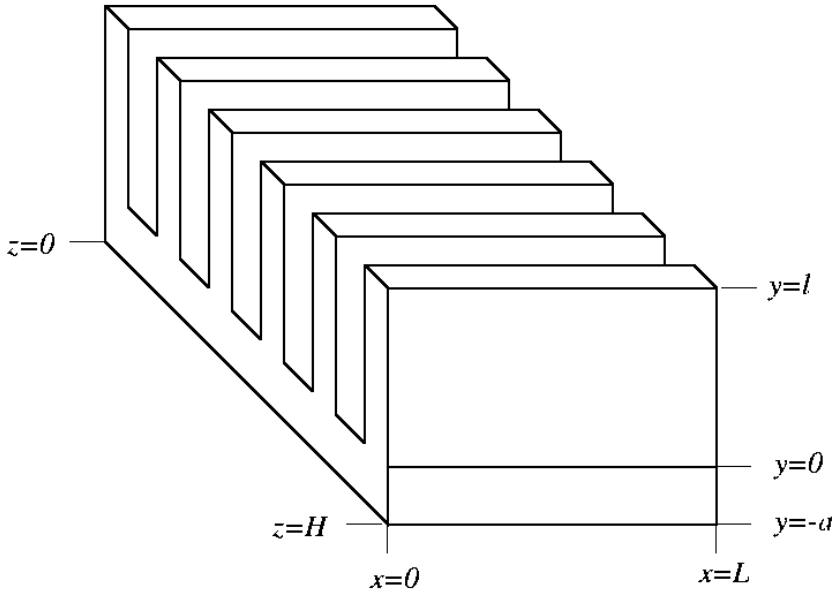

Figure 1.1: Schematic view of heat sink.

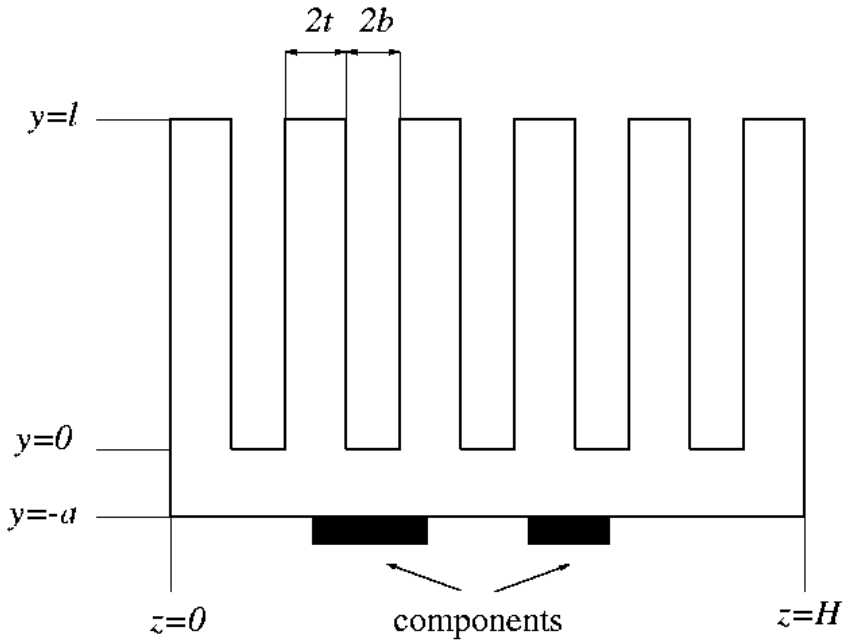

Figure 1.2: Schematic front view of heat sink.

as a function of the temperature of the components, the outflow temperature, the outer dimensions and the noise. There are numerous design parameters that affect the issues to be minimised. The operation of the simple-looking heat sink consisting of rectangular plate fins is affected by the following parameters:

- Base plate thickness a
- Heat sink length L
- Heat sink width H
- Fin length l
- Fin thickness $2t$
- Fin spacing $2b$
- Choice of fin, base plate and fluid materials
- Properties of fan or pump
- Placement of component(s)

From the heat transfer point of view, the most interesting thing is to determine the temperature of the components for a given heat sink design. This is a difficult problem that can be approached with many different ways. The most convenient for the designer would be an analytical formula or an empirical correlation relating the design parameters and the maximum temperature of the system. The multitude of the design parameters and the complexity of the heat transfer problems suggest that finding a formula that realistically describes the physics of the case is very difficult.

The second alternative is to calculate the case with the help of computational fluid dynamics software. This alternative is becoming increasingly attractive as the cost of extensive computing diminishes. However, the method has its drawbacks. In order to obtain reliable results, one needs to have the control volumes or nodes very densely spaced in the gaps between the fins. This results in a relatively large computational effort. In addition, the computational grid has to be regenerated each time the heat sink design is changed. This makes the use of the computational fluid dynamics less attractive at the optimisation stage. Furthermore, the coupling between conduction and convection may cause convergence problems during the computations.

The third alternative is manufacturing prototypes and carrying out measurements on them. If the measurements are done correctly, they can give very valuable information about the operation of the prototype. However, this is very slow and expensive, which makes the method unsuitable for the early design process. Furthermore, analysis is always needed to complement measurements in order to improve the prototype.

There is plenty of literature on forced convection between parallel plates. Analytical methods for optimising the plate spacing in an isothermal heat sink have been developed in [Bejan & Sciubba], [Mereu et al.], [Bejan & Morega]. They used the method of intersecting asymptotes, which provides an analytical formula for the optimal plate spacing in various different flow conditions. For electronics cooling, the most realistic choice for the flow condition they cover is the assumption of prescribed available pumping power. This is a very realistic assumption for a fan operating near its best efficiency point.

The method can be expected to give fairly accurate results also in the non-isothermal case. However, the method cannot be used to calculate the total heat flux transferred by the heat sink. Moreover, as the optimisation is done only for the plate spacing, the method gives no information on how to choose the remaining heat sink dimensions.

Fin spacing optimisation has also been done from the conduction point of view for fins of various different shapes [Yeh & Chang]. However, it was assumed that the base plate is isothermal and that the heat transfer coefficient is spatially uniform. Moreover, the convective heat transfer coefficient was assumed to be independent on the fin spacing, which is clearly inaccurate for densely spaced fins.

On the other hand, a lot of research has been done on conduction in the base plate with discrete heat sources attached at the bottom of the base plate [Culham & Yovanovich], [Lee et al.], [Yovanovich et al.], [Muzychka et al. 2003], [Muzychka et al. 2004]. In these papers, the top of the base plate was assumed to be cooled by a uniform convective heat transfer coefficient or a uniform effective heat transfer coefficient, which can be calculated from the fin-side thermal resistance. It was explicitly or implicitly assumed that the fin-side thermal resistance can be calculated using the one-dimensional fin theory. Furthermore, the base plate spreading resistance and the fin-side thermal resistance were assumed to operate in series.

In reality, the assumption of the base plate and fin-side thermal resistances to be in series is not always valid. As pointed out in [Lehtinen & Karvinen 2004], the spreading of the heat not only happens in the base plate, but in the x-direction also in the fins. For thick enough fins, this may have a significant effect in diminishing the total thermal resistance of the heat sink.

There seems to have been quite a lot interest in two-dimensional fins, where the conduction in the y- and z-directions are treated [Ma et al.], [Buikis et al.]. However, there exist considerably less papers on two-dimensional fins with conduction in the y- and x-directions. Perhaps the reason is that for a uniform heat transfer coefficient, the total heat transfer rates given by one-dimensional and two-dimensional analyses coincide. However, in the heat sink applications the total amount of heat transferred is not as important as the existence of hot spots in the base plate. Thus, it is very important to know the spatial distribution of the heat flux transferred from the base plate by the fins.

Depending on the heat transfer efficiency, there may by a significant wake effect in the heat sink. Due to the fluid warming, the components near the trailing edge of the heat sink tend to be hotter than the components near the leading edge. Thus, the heat transfer coefficient based on the fluid inlet temperature is actually non-uniform. The wake effect for a plate has been analysed in [Culham et al.], [da Silva et al.].

There is also plenty of analysis for one-dimensional and two-dimensional fins with a variable heat transfer coefficient [Ünal], [Ma et al.]. In these papers the heat transfer coefficient was a prescribed function depending either on location ($h = h(y)$) or the local fin temperature ($h = h(T_f)$). Also vapour condensation in fins has been taken into account, which is an important phenomenon in air conditioning, but of no interest in heat sink design [Karvinen et al.].

However, the heat transfer coefficient in the heat sinks is not a function that would be known *a priori*. Instead, the spatially variable heat transfer coefficient needs to be determined as a solution for a conjugated convection and conduction problem. These kind of conjugated solutions have been found for a single fin [Karvinen] and for an array of fins cooled by forced convection [Lehtinen & Karvinen 2005]. However, the applicability of these solutions in realistic heat sink calculations are limited by the facts that the fin base was assumed to be isothermal and that the x-direction conduction was neglected.

In conclusion, analytical methods that consider the plate-fin heat sink as a whole, taking into account the convection in the fins conjugated with the conduction both in the base plate and in the fins, seem to be missing. The goal of this thesis is to obtain a way to calculate the temperature field in a heat sink, taking into account the conjugated convection and conduction heat transfer, but neglecting thermal radiation. The conduction will be treated three-dimensionally in the base plate and two-dimensionally in the fins, assuming that each fin has a uniform temperature in the thickness direction. The purpose is to develop an algorithm with which the solution is accurate, but still markedly easier to compute than with the computational fluid dynamics.

Throughout the thesis, the treatment is maintained as general as possible. There is no limitation for the Reynolds number at which the heat sink is operated. Furthermore, the coolant can be either liquid or gas, as long as $\mathrm{Pr} \geq 0.5$. The physical properties of the base plate are allowed to differ from those of the fins. The number, shape and heat flux distribution of the heat sources are arbitrary. Thermal contact resistance is allowed to occur between the electronic components and the base plate, but the temperature is only solved for the heat sink, not for the electronic components.

However, perfect thermal contact is assumed between the base plate and the fins. In addition, the treatment is limited to shrouded heat sinks. In other words, there is no by-pass flow. It is also assumed that the heat conductivities of the base plate and the fins are much larger than that of the coolant fluid. Furthermore, it is assumed that the fin thickness and spacing, $2t$ and $2b$, are much smaller than the

other heat sink dimensions, L, H and l. The base plate thickness a is assumed to be at least of the same order of magnitude as the fin spacing $2b$.

1.2 Organisation of the thesis

In Chapter 2, the most important issues of the one-dimensional fin theory are reviewed. Also commonly used results for forced convection between parallel plates are given. Moreover, coupling the fin theory and the convection results together is discussed. In Chapter 3, the base plate temperature is solved using the method of effective heat transfer coefficient, which can be found in the literature. In Chapter 4, the traditional fin theory is extended by allowing two-dimensional conduction in the fins. In Chapter 5, the analysis of the fins is further complicated by using a more realistic convection model than what is done in the traditional fin theory.

In Chapter 6, the base plate temperature is solved by using the results for the heat transfer in the fins, which were developed in Chapter 4 and Chapter 5. In Chapter 7, some numerical examples are examined and the results given by the different calculation methods are compared. The calculation methods and the results they give are further discussed in Chapter 8. Finally, the conclusions are given in Chapter 9.

The Fourier cosine series and some related properties of the cosine function are reviewed in Appendix A. To improve the readability of the text, some integrals occurring in the development of the theory are given in Appendix B. Definitions of some matrix functions used in the thesis are given in Appendix C. Also the numerical computation of the relevant matrix functions is discussed.

Chapter 2

Preliminaries

2.1 Fin theory

Extended surfaces play a vital role in numerous heat transfer applications. They are used to enhance heat transfer by providing a much larger heat transfer surface than what would be obtained without them. The traditional analysis of extended surfaces is based on the so-called Murray–Gardner assumptions [Kraus, pp. 3–4], which are:

1. The heat flow in the fin and the temperature at any point on the fin remain constant with time
2. The fin material is homogeneous and its thermal conductivity is the same in all directions and remains constant.
3. The heat transfer coefficient between the fin and the surrounding medium is uniform and constant over the entire surface of the fin.
4. The temperature of the medium surrounding the fin is uniform
5. The fin width is so small compared with its height that temperature gradients across the fin width may be neglected.
6. The temperature at the base of the fin is uniform
7. There are no heat sources within the fin itself
8. Heat transfer to or from the fin is proportional to the temperature excess between the fin and the surrounding medium
9. There is no contact resistance between fins in the configuration or between the fin at the base of the configuration and the prime surface.
10. The heat transferred through the outermost edge of the fin (the fin tip) is negligible compared to that through the lateral surfaces (faces) of the fin.

Naturally, in practise there exist plenty of situations where none of these idealised assumptions are valid. However, the assumptions offer the basis for simple analytical treatment of heat transfer in extended surfaces. It can easily be shown that the Murray–Gardner assumptions imply the following equation governing the temperature excess of the fin

$$k_f t \frac{d^2\theta_f}{dy^2} = q(x,y) \tag{2.1}$$

where the heat flux at the right hand side of the equation is calculated from

$$q(x,y) = h\theta_f(x,y) \tag{2.2}$$

The boundary conditions for Eq. (2.1) are $\theta(x,0) = \theta_b$ and $\left.\frac{d\theta}{dy}\right|_{y=l} = 0$. The solution of Eqs. (2.1) and (2.2) is derived in numerous text books, for example [Incropera & DeWitt, p. 126]:

$$\frac{\theta_f(x,y)}{\theta_b} = \frac{\cosh\left(m(l-y)\right)}{\cosh(ml)} \tag{2.3}$$

where

$$m = \sqrt{\frac{h}{k_f t}} \tag{2.4}$$

Differentiating Eq. (2.3) at the base of the fin yields the total heat rate transferred by the heat sink

$$Q = \frac{k_f m t L H \theta_b}{t+b} \tanh(ml) \tag{2.5}$$

where the number of the fins in the heat sink has been approximated with

$$N_f = \frac{H}{2(t+b)} \tag{2.6}$$

The fin-side thermal resistance $R_{fins} = \theta_b/Q$ can be solved from Eq. (2.5) as

$$R_{fins} = \frac{t+b}{k_f m t L H \tanh(ml)} \tag{2.7}$$

The power of the Murray–Gardner assumptions lies in the simple results in Eqs. (2.3) and (2.5) that they imply. However, in practise there are numerous situations where using the Murray–Gardner assumptions leads to severe loss of accuracy in the computations. In this thesis, instead of using the Murray–Gardner assumptions numbered 3, 4, 6 and 8, the convective heat transfer will be modelled more accurately and the fin base temperature will be allowed to vary in the x-direction. All the other Murray–Gardner assumptions listed above will be assumed to be valid throughout the thesis. Naturally these assumptions may also be invalid in many practical situations, but these cases are outside of the scope of this thesis.

2.2 Laminar forced convection between parallel plates

For fully developed temperature and velocity profiles in laminar flow between two isothermal plates, it is possible to obtain an analytical solution [Kays et al., p. 89]. However, since the effect of the entrance region is appreciable even for relatively narrow plate spacing, this solution may significantly underestimate heat transfer. Thus, it is more prudent to use an empirical correlation which takes the entrance region into account. The most widely used formula is probably that of Stephan, given in [Shah & London, p. 190]

$$\mathrm{Nu}_m = 7.55 + \frac{0.024\,(L^+/2)^{-1.14}}{1 + 0.0358\,(L^+/2)^{-0.64}\,\mathrm{Pr}^{0.17}} \tag{2.8}$$

where L^+ is the dimensionless length of the heat sink defined by

$$L^+ = \frac{L}{2b\mathrm{RePr}} \tag{2.9}$$

and the mean Nusselt number Nu_m is defined by

$$\mathrm{Nu}_m = \frac{4b}{k_a L}\int_0^L \frac{q(x,y)}{\theta_f(x,y) - \theta_m(x,y)}\,dx \tag{2.10}$$

where

$$\theta_m(x,y) = \frac{1}{bU}\int_0^b u(x,y,z)\,[T_a(x,y,z) - T_\infty]\;dz \tag{2.11}$$

is the mixed mean temperature of the fluid. Note that the definition of the mean Nusselt number in Eq. (2.10) actually implies that the mean Nusselt number Nu_m

is a function of the y-coordinate. However, the correlation in Eq. (2.8) implies that there is no y-dependence.

Also analytical treatments that take the entrance region into account have been presented. For example, an analytical composite model for convection between isothermal parallel plates was proposed in [Teertstra et al.]. The model has only a single empirical parameter, whose value was determined with the help of computational fluid dynamics. The numerical results are very close to those given by Eq. (2.8), at least for $\mathrm{Pr} = 0.7$.

The method proposed by Teertstra is physically much more sound than the fully empirical correlation in Eq. (2.8). However, the drawback is that the present author does not know any correspondent to the model proposed by Teertstra in the turbulent case. Thus, the concept of Nusselt mean number is needs to be introduced in the thesis. To avoid multiple different convective heat transfer concepts, and to keep the treatment as compact as possible, the correlations in Eqs. (2.8)–(2.11) are preferred in this thesis when average heat transfer coefficients are assumed.

However, the heat transfer coefficient for laminar flows is strongly dependent on the temperature boundary condition. The results presented above are only valid for isothermal surfaces. For example, in the fully developed flow with uniform heat flux from the surfaces, the Nusselt number is about 10% higher than in the isothermal case [Shah & London, pp. 155–156].

For conjugated conduction and convection problems, where the temperature and the heat flux distributions of the fins are not known *a priori*, no exact analytical solutions are available. However, the problem lends itself to analytical treatment when some approximations are employed. A commonly used approximation is that of *hydrodynamically fully developed flow*.

Assuming a fully developed velocity profile between two parallel plates and that conduction in the fluid occurs only in the direction normal to the plates (z-direction), the classical Graetz solution is obtained. The result for isothermal parallel plates is [Kays et al., p. 102]

$$q(x, y) = \frac{k_a \theta_f}{b} \sum_{n=0}^{\infty} G_n \exp\left(-\lambda_n^2 x^+\right) \tag{2.12}$$

where

$$x^+ = \frac{x}{2b\mathrm{RePr}} \tag{2.13}$$

is the dimensionless length variable. The coefficients G_n and the eigenvalues λ_n in Eq. (2.12) are given in Table 2.1. The result given by Eq. (2.12) is much more accurate than the result that would have been obtained by assuming also fully

n	λ_n	G_n
0	3.885	1.717
1	13.09	1.139
2	22.32	0.952
> 2	$16\sqrt{\frac{n}{3}} + \frac{20}{3}\sqrt{\frac{1}{3}}$	$2.68\lambda_n^{-1/3}$

Table 2.1: Graetz infinite-series-solution eigenvalues and coefficients for isothermal parallel plates.

developed temperature profile. However, the result still slightly underestimates the heat transfer, especially for small values of x^+, due to the assumption of hydrodynamically fully developed flow.

Since the solution in Eq. (2.12) is linear with respect to the surface temperature, the superposition principle can be used to obtain a solution for arbitrarily varying surface temperature. Assuming that the fin temperature excess function $\theta_f(x^+, y)$ is everywhere differentiable with respect to x^+, the solution in [Kays et al., pp. 112] is obtained

$$q(x,y) = \frac{k_a}{b} \sum_{n=0}^{\infty} G_n \left(\exp(-\lambda_n^2 x^+)\theta_f(0,y) + \int_0^{x^+} \exp\left[-\lambda_n^2 (x^+ - \xi)\right] \frac{\partial \theta_f(\xi, y)}{\partial \xi} d\xi \right) \tag{2.14}$$

The assumption of a fully developed velocity profile is never valid near the entrance region of the heat sink. However, for liquids having a high Prandtl number ($\mathrm{Pr} \geq 5$), the solution in Eq. (2.14) is very accurate. For gases with $\mathrm{Pr} \approx 1$, the Graetz solution underestimates heat transfer. However, the solution in Eq. (2.14) can be used as an approximation even for gases if x^+ is high enough. Although approximate, Eq. (2.14) is frequently preferable over Eq. (2.8) due to the possibility to take the variable surface temperature into account.

2.3 Turbulent forced convection between parallel plates

In the turbulent case there are no analytical convective heat transfer solutions. Thus, the designer needs to rely on the available experimental data. However, from the point of view of conjugated heat transfer problems, turbulent flows are much easier to treat than laminar ones. This is because of the fact that the heat transfer coefficient is virtually independent on the temperature boundary condition [Hewitt, p. 2.5.1-5].

Consequently, complexities like the integral equation (2.14) can be safely avoided in the turbulent case by simply assuming a uniform heat transfer coefficient.

Moreover, the heat transfer is also nearly independent on the shape of the duct cross section. This allows one to use the results of circular ducts also in the case of parallel plates, as long as the duct diameter is replaced with the hydraulic diameter $d_h = 4b$.

There are numerous experimental correlations for turbulent forced convection in ducts. For example, Gnielinski proposed the following formula [Hewitt, p. 2.5.1-5]

$$\mathrm{Nu}_m = \frac{(c_f/8)(\mathrm{Re} - 1000)\mathrm{Pr}}{1 + 12.7\sqrt{c_f/8}(\mathrm{Pr}^{2/3} - 1)} \left[1 + \left(\frac{4b}{L}\right)^{2/3}\right] \tag{2.15}$$

where the friction factor c_f may, for smooth surfaces, be calculated from

$$c_f = (1.82 \log_{10}(\mathrm{Re}) - 1.64)^{-2} \tag{2.16}$$

2.4 Simple isothermal heat sink

Writing a differential energy balance and using the definition of the fluid mixed mean temperature in Eq. (2.11) gives the result

$$q(x, y) = \rho c_p b U \frac{\partial \theta_m}{\partial x} \tag{2.17}$$

The simplest way to evaluate the thermal performance of a heat sink is to assume that both the base plate and the fins are isothermal. Assuming a constant surface temperature $\theta_f(x, y) = \theta_b$ and using the definition of the Nusselt number, Eq. (2.10), together with Eq. (2.17) yields the solution [Shah & London, p. 59]

$$\epsilon = 1 - e^{-N_{tu}} \tag{2.18}$$

where the heat sink effectiveness ϵ is defined as a ratio of the total heat transfer rate and the maximum possible heat transfer rate with the given mass flow rate

$$\epsilon = \frac{Q}{\dot{m} c_p \theta_f} \tag{2.19}$$

and N_{tu} is the number of transfer units defined by

$$N_{tu} = \frac{h_m L}{\rho c_p b U} \tag{2.20}$$

where the heat transfer coefficient h_m is defined by

$$h_m = \frac{\mathrm{Nu}_m k_a}{4b} \tag{2.21}$$

It may easily be checked that assuming

$$q(x, y) = h_m \left[\theta_f(x, y) - \theta_m(x, y)\right] \tag{2.22}$$

and using Eq. (2.17) also results in Eq. (2.19) in the case of isothermal fins. In view of this, h_m will be called the *heat transfer coefficient based on mixed mean flow temperature*, in order to distinguish it from h in Eq. (2.2), which is the *heat transfer coefficient based on fluid inlet temperature*.

The assumption of an isothermal heat sink is very seldom adequate. Usually, the base plate cannot be assumed to be isothermal, because the areas where the components are attached are much hotter than the other parts of the base plate [Incropera, p. 19]. Moreover, as shown in Section 2.1, the fins are isothermal only if they are very thick. Thus, variable surface temperature needs to be taken into account either with the simple fin theory or using a more detailed conjugated analysis, as will be done later in the thesis.

2.5 Combining convection and fin theory

In reality, many of the Murray–Gardner assumptions are not strictly valid. However, the result they imply, namely the total heat transfer rate given by Eq. (2.5), may be used as an approximation in many cases. The only question when using Eq. (2.5) is the correct choice of the heat transfer coefficient h in Eq. (2.4). In the laminar case, a way to do this using a composite convection model is presented in [Teertstra et al.]. However, in the turbulent case, or when the more commonly used laminar convection result in Eq. (2.8) is preferred to be used, a different approach is needed.

It is clear that setting $h = h_m$ would overestimate heat transfer as Eq. (2.2) defines h to be the heat transfer coefficient based on the fluid inlet temperature while Eq. (2.22) shows that h_m is the heat transfer coefficient based on the mixed mean flow temperature. It is natural to demand that the fin theory gives correct results in the isothermal case. Assuming $k_f = \infty$, using $\dot{m} = \rho U H l \frac{b}{t+b}$ and combining Eqs. (2.5) and (2.18)–(2.20) yields

$$h = \frac{h_m}{N_{tu}} \left(1 - e^{-N_{tu}}\right) \tag{2.23}$$

Examining Eq. (2.23) shows that for very short heat sinks ($N_{tu} \ll 1$), the equation reduces to $h \approx h_m$. Physically, this means that the warming of the fluid in the x-direction is of no importance, and that the heat transfer coefficients based on

the fluid inlet temperature and the fluid mixed mean temperature coincide. On the other hand, for very long heat sinks ($N_{tu} \gg 1$), the heat transfer coefficient h based on the fluid inlet temperature tends to zero. Physically, this means that increasing heat sink length produces very little additional heat transfer rate, since the fluid has already warmed to the heat sink temperature.

Using Eq. (2.23) together with Eq. (2.5) and the convection results presented in Section 2.2 and Section 2.3 is expected to give reasonable results. In the laminar case with $\mathrm{Pr} = 0.7$, the results are essentially similar to those given in [Teertstra et al.].

This far, however, no attempt has been to model the effect of the non-isothermal base plate or the conjugated conduction and convection in the fins. These effects will be treated in the following chapters.

Chapter 3

Conduction in base plate

Consider the heat sink shown in Figs. 1.1 and 1.2. The heat sink consists of a base plate and a number of fins. There is a number of heat sources attached to the bottom of the heat sink. It is assumed that the heat fluxes of the electronic components are known *a priori*. They can be either uniform or spatially distributed. Thus, the heat flux at the bottom of the base plate can be described with a function $q(x, z)$. Furthermore, it is assumed that the heat leaves the base plate only through the fins. In other words, the base plate edges, the fin edges, the gaps between the fins at the top of the base plate and the gaps between the components at the bottom of the base plate are assumed to be insulated. Moreover, thermal radiation is assumed to be negligible.

In this chapter, only conduction in the base plate is treated while the fins are modelled with the assumption of a uniform effective heat transfer coefficient. This can be viewed as the state-of-the-art analytical method for heat sink calculations. The analysis has been previously carried out by [Muzychka et al. 2003], but it is repeated here with a slightly different formulation that is more suitable for the purposes of the following chapters. In particular, the origin of the y-axis is taken to be at the top of the base plate in order to have a more natural boundary condition for the fins in the following chapters.

The steady-state temperature of the base plate with constant thermal conductivity is governed by the heat equation [Incropera & DeWitt, p. 56]

$$\frac{\partial^2 \theta_b}{\partial x^2} + \frac{\partial^2 \theta_b}{\partial y^2} + \frac{\partial^2 \theta_b}{\partial z^2} = 0 \tag{3.1}$$

The temperature distribution in the base plate can be presented in the form of Fourier cosine series, see Appendix A

$$\theta_b(x, y, z) = \sum_{i=0}^{\infty} \sum_{j=0}^{\infty} \theta_{b,ij}(y) \cos(\alpha_i x) \cos(\beta_j z) \tag{3.2}$$

where $\alpha_i = i\pi/L$ and $\beta_j = j\pi/H$. It is noted that Eq. (3.2) automatically satisfies the adiabatic boundary conditions at the edges of the base plate. Substituting Eq. (3.2) into the heat equation, Eq. (3.1), multiplying the resulting equation by $\cos(\alpha_i x)\cos(\beta_j z)$ and integrating in the x- and z-directions over the entire base plate, yields an ordinary differential equation for each $\theta_{b,ij}(y)$

$$\frac{d^2\theta_{b,ij}}{dy^2} = \gamma_{ij}^2 \theta_{b,ij} \tag{3.3}$$

where $\gamma_{ij}^2 = \alpha_i^2 + \beta_j^2$. The solution of Eq. (3.3) is straightforward, but one needs to notice the special form of solution for the case $i = j = 0$, which arises due to the zero eigenvalue. The general form of the solution for the base plate temperature distribution obtained from Eqs. (3.2)–(3.3) is given by

$$\theta_b = A_{00} + B_{00}y + \sum_{\substack{i=0 \\ i+j\neq 0}}^{\infty}\sum_{j=0}^{\infty}\left[A_{ij}\cosh(\gamma_{ij}y) + \frac{B_{ij}}{\gamma_{ij}}\sinh(\gamma_{ij}y)\right]\cos(\alpha_i x)\cos(\beta_j z) \tag{3.4}$$

The coefficients A_{ij} and B_{ij} need to be determined from the boundary conditions at the bottom of the base plate and at the junction between the base plate and the fins. The bottom boundary condition is the simpler of the two, and it is treated first. The heat flux at the bottom of the base plate can be obtained by differentiating Eq. (3.4) at $y = -a$

$$\begin{aligned} q(x,z) &= -k_b \left.\frac{\partial\theta_b}{\partial y}\right|_{y=-a} \\ &= k_b \sum_{i=0}^{\infty}\sum_{j=0}^{\infty}\left[\gamma_{ij}\sinh(\gamma_{ij}a)A_{ij} - \cosh(\gamma_{ij}a)B_{ij}\right]\cos(\alpha_i x)\cos(\beta_j z) \end{aligned} \tag{3.5}$$

where the symmetry property of the hyperbolic cosine

$$\cosh(-\gamma_{ij}a) = \cosh(\gamma_{ij}a)$$

and the anti-symmetry property of the hyperbolic sine

$$\sinh(-\gamma_{ij}a) = -\sinh(\gamma_{ij}a)$$

have been used [Spanier & Oldham, p. 264]. Using the orthogonality property of the cosine function, Eq. (A.2), one can rewrite Eq. (3.5) as

$$k_b\left[\gamma_{ij}\sinh(\gamma_{ij}a)A_{ij} - \cosh(\gamma_{ij}a)B_{ij}\right] = Q_{ij} \tag{3.6}$$

where

$$Q_{ij} = \frac{\int_0^L \int_0^H q(x,z) \cos(\alpha_i x) \cos(\beta_j z) \; dz \; dx}{\int_0^L \int_0^H \cos^2(\alpha_i x) \cos^2(\beta_j z) \; dz \; dx} \tag{3.7}$$

The coefficients Q_{ij} are the Fourier coefficients of the bottom heat flux $q(x,z)$ and they can be readily calculated for any prescribed heat flux distribution. To be able to solve A_{ij} and B_{ij}, one needs an additional equation relating them. This can be obtained by imposing a boundary condition at the junction between the base plate and the fins at $y = 0$. In the literature, the most commonly used boundary condition is a uniform effective heat transfer coefficient at the top of the base plate [Muzychka et al. 2003]

$$-k_b \left. \frac{\partial \theta_b}{\partial y} \right|_{y=0} = h_{eff} \theta_b(x,0,z) \tag{3.8}$$

where

$$h_{eff} = \frac{1}{LHR_{fins}} \tag{3.9}$$

and the simplest way to calculate the fin-side thermal resistance R_{fins} is given in Eq. (2.7).

Using Eqs. (3.4) and (3.8) together with the orthogonality property of the cosine function, Eq. (A.2), yields

$$-k_b B_{ij} = h_{eff} A_{ij} \tag{3.10}$$

The final solution can now be obtained by solving the coefficients A_{ij} and B_{ij} from Eqs. (3.6) and (3.10)

$$A_{ij} = \frac{Q_{ij}}{k_b \gamma_{ij} \sinh(\gamma_{ij} a) + h_{eff} \cosh(\gamma_{ij} a)} \tag{3.11a}$$

$$B_{ij} = -\left[\frac{k_b \gamma_{ij}}{h_{eff}} \sinh(\gamma_{ij} a) + \cosh(\gamma_{ij} a) \right]^{-1} \frac{Q_{ij}}{k_b} \tag{3.11b}$$

The base plate temperature distribution can now be calculated by substituting Eq. (3.11) into Eq. (3.4). The result coincides to that presented in [Muzychka et al. 2003]. If desired, the temperature distribution given by Eq. (3.4) can easily be averaged over the heat source area to obtain the average temperature of the junction between the base plate and the component.

If the effective heat transfer coefficient h_{eff} is calculated using Eqs. (2.7) and (3.9), the result in Eq. (3.11) can be rewritten as

$$A_{ij} = \frac{Q_{ij}}{k_b \left[\gamma_{ij} \sinh(\gamma_{ij} a) + rm \tanh(ml) \cosh(\gamma_{ij} a)\right]} \tag{3.12a}$$

$$B_{ij} = -\left[\frac{\gamma_{ij} \sinh(\gamma_{ij} a)}{rm \tanh(ml)} + \cosh(\gamma_{ij} a)\right]^{-1} \frac{Q_{ij}}{k_b} \tag{3.12b}$$

where $r = \frac{k_f t}{k_b(t+b)}$ is a dimensionless fin thickness parameter. The result in Eq. (3.12) is in a more convenient form than Eq. (3.11) for the purpose of comparisons between this result and the ones presented later in the thesis.

Chapter 4

Fin theory with conduction in flow direction

The solution presented in Chapter 3 treats the conduction only in the base plate and approximates the effect of the fins as a uniform effective heat transfer coefficient imposed at the top of the base plate. This approach is simple and often adequate to obtain reasonable results. However, the treatment neglects some physical phenomena, such as deterioration of the heat transfer coefficient toward the trailing edge of the heat sink and the conduction in the fins in the x-direction.

In the following, the purpose is to establish a solution for the heat sink taking the two-dimensional conduction in the fins into account. The heat transfer coefficient from the fins to the ambient air is assumed to be a constant h. Each of the fins is assumed to be so thin, that the conduction in the z-direction can be neglected. Moreover, the heat flux through the edges and the tips of the fins is assumed to be negligible.

Thus, the temperature distribution in a single fin can be modelled with the equation

$$k_f t \left(\frac{\partial^2 \theta_f}{\partial x^2} + \frac{\partial^2 \theta_f}{\partial y^2} \right) = q(x, y) \tag{4.1}$$

where

$$q(x, y) = h\theta_f(x, y) \tag{4.2}$$

The boundary condition at the base of the fin is a prescribed arbitrary temperature function $\theta_f(x, 0)$. For the fin tip, the customary boundary condition of negligible heat flux is used

$$\left.\frac{\partial \theta_f}{\partial y}\right|_{y=l} = 0 \tag{4.3}$$

The temperature distribution in the fin can be presented in the form of Fourier cosine series

$$\theta_f(x,y) = \sum_{i=0}^{\infty} \theta_{f,i}(y) \cos\left(\alpha_i x\right) \tag{4.4}$$

The adiabatic boundary conditions at $x = 0$ and $x = L$ are automatically satisfied by fin temperature in Eq. (4.4). Substituting the series in Eq. (4.4) into Eqs. (4.1) and (4.2), multiplying the resulting equation by $\cos\left(\alpha_i x\right)$ and integrating in the x-direction over the entire length of the fin, yields an ordinary differential equation for each $\theta_{f,i}(y)$

$$\frac{d^2\theta_{f,i}}{dy^2} = \mu_i^2 \theta_{f,i} \tag{4.5}$$

where $\mu_i^2 = m^2 + \alpha_i^2$. Solving Eq. (4.5) and substituting the result in Eq. (4.4) yields the general solution for the fin temperature

$$\theta_{f,i}(x,y) = \sum_{i=0}^{\infty} \left[C_i \cosh(\mu_i y) + D_i \sinh(\mu_i y)\right] \cos(\alpha_i x) \tag{4.6}$$

The coefficients C_i and D_i need to be determined from the boundary conditions. Using Eqs. (4.3) and (4.6) together with the orthogonality property of the cosine function, Eq. (A.2), gives a relation between the coefficients C_i and D_i

$$D_i = -\tanh(\mu_i l) C_i \tag{4.7}$$

Using Eq. (4.6) and the orthogonality property of the cosine function, Eq. (A.2), the coefficients C_i can be determined from the base temperature of the fin

$$C_i = \frac{\int_0^L \theta_f(x,0) \cos(\alpha_i x)\ dx}{\int_0^L \cos^2(\alpha_i x)\ dx} \tag{4.8}$$

Finally, using Eqs. (4.4), (4.6), (4.7) and (4.8) yields the relationship between the fin base heat flux and the fin base temperature

$$-k_f \left.\frac{\partial \theta_f}{\partial y}\right|_{y=0} = k_f \sum_{i=0}^{\infty} \mu_i \tanh(\mu_i l) \frac{\int_0^L \theta_f(x,0) \cos(\alpha_i x)\ dx}{\int_0^L \cos^2(\alpha_i x)\ dx} \cos(\alpha_i x) \tag{4.9}$$

The result in Eq. (4.9) is the solution for the heat flux distribution at the base of a single fin with arbitrarily varying fin base temperature $\theta_f(x, 0)$. Section 6.2 shows how to combine this result with conduction in the base plate to obtain the base plate temperature distribution.

Chapter 5

Conjugated heat transfer in fins

In the preceding chapter, the convection was calculated assuming a uniform heat transfer coefficient based on the difference between the fin and the fluid *inlet* temperatures, Eq. (4.1). In practise, this is not always a good assumption. The assumption of a uniform heat transfer coefficient based on the inlet temperature neglects the effect of fluid warming in the x-direction.

The solution Eq. (4.9) in the last chapter implies that a uniform temperature at the fin base produces uniform heat flux at the fin base. Thus, a symmetrically heated base plate would have a symmetrical temperature distribution. The same phenomenon occurs when using the method of effective heat transfer coefficient, Eq. (3.11).

In reality, the temperature maximum in a symmetrically heated base plate occurs at $x > \frac{L}{2}$ because of the fluid warming. The effect may be substantial, since the number of heat transfer units N_{tu} defined by Eq. (2.20) may in practise be in the order of magnitude of 1.

This wake effect was also discussed in [Muzychka et al. 2003] in context of the method of effective heat transfer coefficient. They proposed replacing the boundary condition at the top of the base plate in Eq. (3.8) with

$$-k_b \left.\frac{\partial \theta_b}{\partial y}\right|_{y=0} = h_{eff}\left[\theta_b(x,0,z) - \theta_m(x)\right] \tag{5.1}$$

where the mixed mean temperature excess would be approximated from

$$\theta_m(x) = \frac{Qx}{\dot{m} c_p L} \tag{5.2}$$

where Q is the total heat transfer rate dissipated by the heat sink. However, they did not give any advice on how to use the correction in Eqs. (5.1)–(5.2) to obtain the final solution for the whole base plate temperature distribution. Evidently,

it is no longer possible to obtain a simple closed-form result such as Eq. (3.11). Moreover, it is clear that the approximation in Eq. (5.2) is not very accurate if the bottom heat flux $q(x, z)$ is very non-uniformly distributed over the base plate. Finally, to be precise, the fin theory should also be somehow modified as the warming of the ambient fluid somewhat improves the fin efficiency while decreasing the convective heat transfer rate.

In this chapter, a different approach to the problem is chosen. Instead of using Eqs. (5.1)–(5.2), the two-dimensional temperature field in a single fin is considered like in Chapter 4. However, in this chapter the convection is modelled more accurately than in Chapter 4 in order to take the wake effect into account.

Calculating the convection from Eqs. (2.17) and (2.22) is expected to give more accurate results than Eq. (4.2). In other words, a uniform heat transfer coefficient based on the mixed mean temperature of the fluid, rather than the fluid inlet temperature, is assumed. However, even these equations may lead to errors in the case of laminar flow because the local heat transfer coefficient is dependent on the upstream fin temperature distribution as discussed in Section 2.2.

In Section 5.1, the equations governing the fin temperature are formulated as a second-order ordinary vector differential equation, assuming a uniform heat transfer coefficient based on the mixed mean temperature of the fluid. In Section 5.2, the same procedure is followed assuming laminar hydrodynamically fully developed flow. Finally, the fin temperature is solved in Section 5.3 with the assumption of a prescribed fin base temperature distribution. The coupling of the fins to the base plate is postponed until Chapter 6.

5.1 Problem formulation for uniform heat transfer coefficient based on mixed mean temperature

Eliminating the fluid mixed mean temperature from Eqs. (2.17) and (2.22) yields an integral relation between the fin heat flux and temperature distributions

$$q(x,y) = h_m \left(\theta_f(x,y) - \frac{N_{tu}}{L} \int_0^x \exp\left[N_{tu} \left(\frac{\xi - x}{L} \right) \right] \theta_f(\xi, y)\, d\xi \right) \tag{5.3}$$

It can be seen from Eq. (5.3) that the local heat flux is assumed to depend only on the temperature distribution of the fin in question, and not on those of the neighbouring fins. This is because Eq. (2.17) is strictly valid only if there is temperature symmetry at the centreline between the fins.

In reality, the heat flux is slightly dependent on the temperature distributions of the neighbouring fins. However, at the system level, the net effect of asymmetry in

the wall temperatures is very small. The spreading of the heat in the z-direction occurs quite effectively in the base plate. In comparison to this, the convective heat transfer between two neighbouring fins can be neglected and the symmetry boundary condition at the centreline between the fins is justified.

Each of the fins is naturally allowed to have different temperature distribution depending on their location in the z-direction. The temperature distribution of a single fin can again be presented in the form of Fourier cosine series. Substituting Eq. (4.4) into Eq. (4.1) and changing the summation index yields

$$\sum_{I=0}^{\infty} k_f t \left(-\alpha_I^2 \theta_{f,I} + \frac{d^2\theta_{f,I}}{dy^2} \right) \cos(\alpha_I x) = q(x,y) \tag{5.4}$$

Multiplying both sides of Eq. (5.4) by $\cos(\alpha_i x)$ and integrating in the x-direction over the length of the fin yields

$$\sum_{I=0}^{\infty} k_f t \left(-\alpha_I^2 \theta_{f,I} + \frac{d^2\theta_{f,I}}{dy^2} \right) \int_0^L \cos(\alpha_I x)\cos(\alpha_i x)\ dx = \int_0^L q(x,y)\cos(\alpha_i x)\ dx \tag{5.5}$$

Using the properties of the cosine function in Eqs. (A.2)–(A.3) and rearranging yields an ordinary differential equation for each $\theta_{f,i}(y)$

$$\frac{d^2\theta_{f,i}}{dy^2} = \alpha_i^2 \theta_{f,i} + \frac{2\int_0^L q(x,y)\cos(\alpha_i x)\ dx}{k_f t L(1+\delta(i))} \tag{5.6}$$

where $\delta(i)$ is the delta function defined by Eq. (A.4). To be able to solve Eq. (5.6), the integral on the right hand side needs to be calculated. Substituting the Fourier cosine series presentation of the fin temperature in Eq. (4.4) into the convection model in Eq. (5.3) yields, with the help of Eq. (B.1),

$$\begin{aligned} q(x,y) =& h_m \sum_{I=0}^{\infty} \theta_{f,I} \left(\cos(\alpha_I x) - \frac{N_{tu}}{L} \int_0^x \exp\left[N_{tu} \left(\frac{\xi - x}{L} \right) \right] \cos(\alpha_I \xi)\ d\xi \right) \\ =& h_m \sum_{I=0}^{\infty} \theta_{f,I} \left(\cos(\alpha_I x) - \frac{N_{tu}\left[N_{tu}\left(\cos(\alpha_I x) - e^{-N_{tu}\frac{x}{L}} \right) + I\pi \sin(\alpha_I x) \right]}{N_{tu}^2 + (I\pi)^2} \right) \\ =& h_m \sum_{I=0}^{\infty} \theta_{f,I} \left(\frac{(I\pi)^2 \cos(\alpha_I x) + N_{tu}^2 e^{-N_{tu}\frac{x}{L}} - N_{tu} I\pi \sin(\alpha_I x)}{N_{tu}^2 + (I\pi)^2} \right) \end{aligned} \tag{5.7}$$

Substituting Eq. (5.7) into Eq. (5.6) and performing the integration on the right hand side with the help of Eqs. (A.2), (A.3), (B.2) and (B.3) gives an ordinary differential equation for each $\theta_{f,i}(y)$

$$\begin{aligned}\frac{d^2\theta_{f,i}}{dy^2} &= \left[\alpha_i^2 + \left(\frac{h_m}{k_f t}\right)\frac{(i\pi)^2}{N_{tu}^2 + (i\pi)^2}\right]\theta_{f,i} \\ &+ \left(\frac{h_m}{k_f t}\right)\left(\frac{2N_{tu}^3}{1+\delta(i)}\right)\left(\frac{1-(-1)^i e^{-N_{tu}}}{N_{tu}^2 + (i\pi)^2}\right)\sum_{I=0}^{\infty}\frac{\theta_{f,I}}{N_{tu}^2 + (I\pi)^2} \\ &+ \left(\frac{h_m}{k_f t}\right)\left(\frac{2N_{tu}}{1+\delta(i)}\right)\sum_{\substack{I=0 \\ I\neq i}}^{\infty}\frac{I^2\left[1-(-1)^{i+I}\right]}{\left[i^2-I^2\right]\left[N_{tu}^2+(I\pi)^2\right]}\theta_{f,I}\end{aligned} \tag{5.8}$$

If the Fourier cosine series in Eq. (4.4) is truncated such that only the functions $\theta_{f,i}$ for $i < N_i$ are considered, Eq. (5.8) gives N_i ordinary differential equations for N_i unknown functions $\theta_{f,i}(y)$. Using matrix notation, Eq. (5.8) can be rewritten as

$$\frac{d^2\boldsymbol{\theta_f}}{dy^2} = \boldsymbol{M}^2\boldsymbol{\theta_f} \tag{5.9}$$

where

$$\boldsymbol{\theta_f}(y) = \left[\theta_{f,0}(y)\ \theta_{f,1}(y)\ ...\ \theta_{f,N_i-1}(y)\right]^T \tag{5.10}$$

and the elements of the matrix $\boldsymbol{M}^2 = \{{M^2}_{iI}\} \in \mathbb{R}^{N_i \times N_i}$ may be found by examining Eq. (5.8). The matrix $\boldsymbol{M}^2$ appears as squared in Eq. (5.9) to maintain the treatment analogous to the one-dimensional fin theory in Section 2.1. The diagonal elements ($i = I, 0 \leq i < N_i$) of the matrix $\boldsymbol{M}^2$ are

$${M^2}_{ii} = \alpha_i^2 + \frac{h_m}{k_f t}\left[\frac{(i\pi)^2}{N_{tu}^2 + (i\pi)^2} + \left(\frac{2N_{tu}^3}{1+\delta(i)}\right)\left(\frac{1-(-1)^i e^{-N_{tu}}}{\left[N_{tu}^2 + (i\pi)^2\right]^2}\right)\right] \tag{5.11a}$$

and the non-diagonal elements ($i \neq I, 0 \leq i < N_i, 0 \leq I < N_i$) of the matrix $\boldsymbol{M}^2$ are

$${M^2}_{iI} = \frac{h_m}{k_f t}\left(\frac{2N_{tu}}{1+\delta(i)}\right)\left[\frac{N_{tu}^2\left[1-(-1)^i e^{-N_{tu}}\right]}{\left[N_{tu}^2+(i\pi)^2\right]\left[N_{tu}^2+(I\pi)^2\right]} + \frac{I^2\left[1-(-1)^{i+I}\right]}{\left[i^2-I^2\right]\left[N_{tu}^2+(I\pi)^2\right]}\right] \tag{5.11b}$$

It can by seen from Eq. (5.11) that if $N_i = 1$ and the relation between the heat transfer coefficients h and h_m is taken from Eq. (2.23), the matrix $\boldsymbol{M}^2$ reduces to the scalar $\boldsymbol{M}^2 = m^2$. In this case the solution of Eq. (5.9) reduces to the one-dimensional solution in Eq. (2.3). This observation further justifies the choice of the average heat transfer coefficient h in Eq. (2.23).

On the other hand, in the limit of very large mass flow rate, Eq. (2.20) gives $N_{tu} \to 0$. At this limit, Eq. (2.23) gives $h_m \to h$. The matrix $\boldsymbol{M}^2$ in Eq. (5.11) is seen to reduce to a diagonal matrix, whose elements are given by ${M^2}_{ii} = \mu_i^2$. Thus, the set of differential equations in Eq. (4.5) and the solution in Eq. (4.9) are recovered. Consequently, as expected, the effect of fluid warming is negligible for small values of N_{tu}.

However, for large and moderate values of N_{tu}, the full vector differential equation (5.9) is needed. Its solution will be given in Section 5.3.

5.2 Problem formulation for laminar hydrodynamically developed flow

The results obtained by the method presented in Section 5.1 are expected to be fairly accurate for turbulent flows. For laminar flows, however, the assumption of a uniform heat transfer coefficient may lead to errors. In reality, the local heat flux from the fins is dependent on the whole upstream temperature distribution.

The purpose of this section is to present a calculation method for laminar flows. The method is similar to that used in Section 5.1, but now the convection from the fins is modelled differently. The flow is assumed to be hydrodynamically fully developed. This assumption is strictly valid only for fluids with high Prandtl number, but the assumption can also be used for air, at least for dense fin spacing.

In addition, it is assumed that the conduction in the fluid occurs only in the direction normal to the fins (z-direction). Furthermore, temperature symmetry is assumed at the centreline between the fins as explained in Section 5.1.

The above assumptions lead to the integral form of the Graetz solution for convection, which was presented in Eq. (2.14). Substituting the Fourier cosine series form of the fin temperature in Eq. (4.4) into the Graetz solution in Eq. (2.14) and using Eq. (B.4) yields

$$\begin{aligned} q(x,y) &= \frac{k_a}{b} \sum_{n=0}^{\infty} \sum_{I=0}^{\infty} \theta_{f,I} G_n \left(e^{-\lambda_n^2 x^+} + \int_{\xi=0}^{x^+} e^{-\lambda_n^2 (x^+ - \xi)} \frac{\partial \cos\left(\frac{\alpha_I x}{x^+}\xi\right)}{\partial \xi} \, d\xi \right) \\ &= \frac{k_a}{b} \sum_{n=0}^{\infty} \sum_{I=0}^{\infty} \theta_{f,I} G_n \left(e^{-\lambda_n^2 x^+} + \frac{(I\pi)^2 \left[\cos(\alpha_I x) - e^{-\lambda_n^2 x^+}\right] - \lambda_n^2 L^+ I\pi \sin(\alpha_I x)}{\left(\lambda_n^2 L^+\right)^2 + (I\pi)^2} \right) \\ &= \frac{k_a}{b} \sum_{n=0}^{\infty} \sum_{I=0}^{\infty} \theta_{f,I} G_n \left(\frac{(I\pi)^2 \cos(\alpha_I x) + \left(\lambda_n^2 L^+\right)^2 e^{-\lambda_n^2 x^+} - \lambda_n^2 L^+ I\pi \sin(\alpha_I x)}{\left(\lambda_n^2 L^+\right)^2 + (I\pi)^2} \right) \end{aligned} \tag{5.12}$$

Substituting Eq. (5.12) into Eq. (5.6) and performing the integration on the right hand side with the help of Eqs. (A.2), (A.3), (B.3) and (B.5) gives an ordinary differential equation for each $\theta_{f,i}(y)$

$$\begin{aligned}\frac{d^2\theta_{f,i}}{dy^2} &= \left(\alpha_i^2 + \frac{k_a}{k_f bt}\sum_{n=0}^{\infty}\frac{G_n(i\pi)^2}{\left(\lambda_n^2 L^+\right)^2 + (i\pi)^2}\right)\theta_{f,i} \\ &+ \frac{k_a}{k_f bt}\sum_{n=0}^{\infty} G_n \frac{2\left(\lambda_n^2 L^+\right)^3}{1+\delta(i)}\left(\frac{1-(-1)^i e^{-\lambda_n^2 L^+}}{\left(\lambda_n^2 L^+\right)^2 + (i\pi)^2}\right)\sum_{I=0}^{\infty}\frac{\theta_{f,I}}{\left(\lambda_n^2 L^+\right)^2 + (I\pi)^2} \\ &+ \frac{k_a}{k_f bt}\sum_{n=0}^{\infty} G_n \frac{2\lambda_n^2 L^+}{1+\delta(i)}\sum_{\substack{I=0\\ I\neq i}}^{\infty}\frac{I^2\left(1-(-1)^{i+I}\right)}{\left[i^2-I^2\right]\left[\left(\lambda_n^2 L^+\right)^2 + (I\pi)^2\right]}\theta_{f,I} \end{aligned} \tag{5.13}$$

Truncating the Fourier cosine series, Eq. (5.13) can again be written in the matrix notation with Eq. (5.9). The only difference to Section 5.1 is that the elements of the matrix $\boldsymbol{M}^2$ are different. This time inspecting Eq. (5.13) gives the diagonal elements of the matrix $\boldsymbol{M}^2$

$${M^2}_{ii} = \alpha_i^2 + \frac{k_a}{k_f bt}\sum_{n=0}^{\infty} G_n\left[\frac{(i\pi)^2}{\left(\lambda_n^2 L^+\right)^2 + (i\pi)^2} + \frac{2\left(\lambda_n^2 L^+\right)^3}{1+\delta(i)}\left(\frac{1-(-1)^i e^{-\lambda_n^2 L^+}}{\left[\left(\lambda_n^2 L^+\right)^2 + (i\pi)^2\right]^2}\right)\right] \tag{5.14a}$$

while the non-diagonal elements of the matrix $\boldsymbol{M}^2$ are given by

$$\begin{aligned}{M^2}_{iI} &= \frac{k_a}{k_f bt}\sum_{n=0}^{\infty} G_n \frac{2\lambda_n^2 L^+}{1+\delta(i)}\times \\ &\left(\frac{\left(\lambda_n^2 L^+\right)^2\left[1-(-1)^i e^{-\lambda_n^2 L^+}\right]}{\left[\left(\lambda_n^2 L^+\right)^2 + (i\pi)^2\right]\left[\left(\lambda_n^2 L^+\right)^2 + (I\pi)^2\right]} + \frac{I^2\left(1-(-1)^{i+I}\right)}{\left[i^2-I^2\right]\left[\left(\lambda_n^2 L^+\right)^2 + (I\pi)^2\right]}\right)\end{aligned} \tag{5.14b}$$

The elements of the matrix $\boldsymbol{M}^2$ can be calculated to desired accuracy by including a suitable number of Graetz solution eigenvalues in the summation.

5.3 Solution for fin temperature

To be able to solve Eq. (5.9), one needs two boundary conditions. At the present stage, the temperature distribution at the base of the fin is assumed to be a known function $\theta_f(x,0)$. Using Eqs. (4.4) and (5.10), the function $\theta_f(x,0)$ can

be described with a set of its Fourier coefficients $\boldsymbol{\theta_f}(0)$, giving the boundary condition

$$\boldsymbol{\theta_f}(y=0) = \boldsymbol{\theta_f}(0) \tag{5.15a}$$

The actual fin base temperature is later determined by coupling the fin temperature distribution to the base plate temperature distribution. The other boundary condition is the assumption of negligible heat flow from the fin tip.

$$\left.\frac{d\boldsymbol{\theta_f}}{dy}\right|_{y=l} = 0 \tag{5.15b}$$

The solution of Eq. (5.9) with the boundary conditions in Eq. (5.15) is

$$\boldsymbol{\theta_f}(y) = (\cosh(\boldsymbol{M}l))^{-1} \cosh\left(\boldsymbol{M}(l-y)\right) \boldsymbol{\theta_f}(0) \tag{5.16}$$

where cosh is the matrix hyperbolic cosine function defined by Eq. (C.3). The validity of the result in Eq. (5.16) may be checked by direct substitution into Eq. (5.9) with the help of the differentiation formulae and commutative properties of the matrix hyperbolic functions in Eqs. (C.6)–(C.7). The matrix $\boldsymbol{M}$ in Eq. (5.16) is any of the square roots of the matrix $\boldsymbol{M}^2$ given by Eqs. (5.11) or (5.14). In other words, $\boldsymbol{M}$ is any matrix such that $\boldsymbol{MM} = \boldsymbol{M}^2$. It can be verified that the solution in Eq. (5.16) reduces to the one-dimensional solution in Eq. (2.3) if $N_i = 1$.

The result is very remarkable. With the knowledge of the base temperature distribution of the fin, one can compute the temperature distribution in the whole fin by taking into account both two-dimensional conduction and using a relatively realistic convection model. In practise, the most interesting issue is the relationship between the fin base temperature and heat flux distributions. This can be obtained by differentiating Eq. (5.16) at the base of the fin

$$-k_f \left.\frac{d\boldsymbol{\theta_f}}{dy}\right|_{y=0} = k_f \boldsymbol{M} \tanh(\boldsymbol{M}l)\boldsymbol{\theta_f}(0) \tag{5.17}$$

where tanh is the matrix hyperbolic tangent function defined by Eq. (C.5). The result in Eq. (5.17) can be rewritten as

$$-k_f \left.\frac{d\boldsymbol{\theta_f}}{dy}\right|_{y=0} = \frac{k_f}{l}\boldsymbol{R}\boldsymbol{\theta_f}(0) \tag{5.18}$$

where

$$\boldsymbol{R} = \boldsymbol{M} l \tanh(\boldsymbol{M} l) \tag{5.19}$$

is a dimensionless matrix. Practical methods for computing the matrix $\boldsymbol{R}$ are given in Appendix C. The heat flux distribution is finally obtained from Eq. (5.18) with the help of Eq. (4.4) and the orthogonality property of the cosine function, Eq. (A.2)

$$\begin{aligned} -k_f \left.\frac{\partial \theta_f}{\partial y}\right|_{y=0} &= -k_f \sum_{i=0}^{N_i-1} \left.\frac{d\theta_{f,i}}{dy}\right|_{y=0} \cos(\alpha_i x) \\ &= \frac{k_f}{l} \sum_{i=0}^{N_i-1} \sum_{I=0}^{N_i-1} R_{iI} \theta_{f,I}(0) \cos(\alpha_i x) \\ &= \frac{k_f}{l} \sum_{i=0}^{N_i-1} \sum_{I=0}^{N_i-1} R_{iI} \frac{\int_0^L \theta_f(x,0) \cos(\alpha_I x)\ dx}{\int_0^L \cos^2(\alpha_I x)\ dx} \cos(\alpha_i x) \end{aligned} \tag{5.20}$$

The result in Eq. (5.20) will be used in Section 6.3 to determine the base plate temperature distribution.

Chapter 6

Solution for base plate temperature

In Chapter 3, the temperature distribution was solved in the whole base plate using the method presented in [Muzychka et al. 2003]. However, a uniform effective heat transfer coefficient was assumed at the top of the base plate. In reality, the things are not quite that simple when a number of fins are attached at the top of the base plate. It should be evident from Chapter 4 and Chapter 5 that the local heat flux at the fin base is not directly proportional to the local base temperature of the fin.

Therefore, the effective heat transfer coefficient in Eq. (3.8) should actually be a non-constant function $h_{eff} = h_{eff}(x, z)$. The variation of the effective heat transfer coefficient occurs due to three different physical phenomena:

- The heat continues to spread in the x-direction in the fins. Therefore, the effective heat transfer coefficient is higher at the relatively hotter areas of the base plate than at the relatively colder areas of the base plate.
- The convective heat transfer rate varies, and generally deteriorates in the x-direction. This causes the effective heat transfer coefficient to behave correspondingly.
- The junction is discontinuous in the z-direction. The effective heat transfer coefficient is very much higher at the bases of the fins than in the gaps between them.

The purpose of this chapter is to treat the top boundary condition of the base plate more rigorously than in Chapter 3 by using the solutions for the fins obtained in Chapter 4 and Chapter 5. However, the discontinuity in the z-direction is still neglected. In Section 6.1, the choice for the boundary condition at the junction between the base plate and the fins is discussed. In Section 6.2, the base plate temperature is solved calculating the heat transfer in the fins with the result

obtained in Chapter 4. In Section 6.3, the fluid warming is taken into account by using the results obtained in Chapter 5.

6.1 Boundary conditions at top of base plate

For simplicity, it is assumed that there is perfect contact between the base plate and the fins. In other words, temperature continuity in the y-direction is assumed at the base of the fin

$$\theta_f(x, 0, z) = \theta_b(x, 0, z) \tag{6.1}$$

The boundary condition in Eq. (6.1) can naturally be applied only at the fin bases, not in the gaps between them. Moreover, the heat flux from the top of the base plate is assumed negligible in the gaps between the fins. In other words, the heat is assumed to leave the base plate only through the fins. This assumption is justified if $b \ll l$. Mathematically, the heat flux at the top of the base plate can be expressed as

$$-k_b \left.\frac{\partial \theta_b}{\partial y}\right|_{y=0} = -k_f g(z) \left.\frac{\partial \theta_f}{\partial y}\right|_{y=0} \tag{6.2}$$

where

$$g(z) = \begin{cases} 1, & \text{for } z \text{ occupied by fin} \\ 0, & \text{for } z \text{ occupied by fluid} \end{cases} \tag{6.3}$$

However, the use of Eqs. (6.2) and (6.3) is quite complicated. A two-dimensional solution for conduction in a fin attached to a base plate has been presented in the form of a Green's function in [Buikis et al.]. However, although the problem is rigorously solved by taking conduction in the y- and z-directions into account, their results are difficult to apply in the present case with non-isothermal base plate in the x-direction. Therefore, in this thesis the heat flux boundary condition is approximated with

$$-k_b \left.\frac{\partial \theta_b}{\partial y}\right|_{y=0} = -\frac{k_f t}{t+b} \left.\frac{\partial \theta_f}{\partial y}\right|_{y=0} \tag{6.4}$$

It can be seen from Eqs. (2.3) and (2.7) that if the one-dimensional fin theory is used, the boundary condition in Eq. (6.4) is identical with the effective heat transfer coefficient boundary condition in Eqs. (3.8)–(3.9).

The approximation in Eq. (6.4) implies that each point at the top of the base plate is thought to be attached to a fin. However, the overall energy conservation

at the junction is guaranteed by reducing the heat flux with the factor $\frac{t}{t+b}$. It can be seen that Eq. (6.4) satisfies Eq. (6.2) in an integral sense. Both equations give the same result if they are integrated in the z-direction over the half-width of a fin and the half-width of the gap adjacent to it.

Physically, the approximation in Eq. (6.4) neglects the constriction resistance of the heat flux leaving the base plate, or the temperature depression of the fin base [Sparrow & Lee]. Therefore, using the approximation overestimates the heat transfer. The effect of the constriction resistance may be substantial for very thin base plate and fins. However, in most of the practical situations its effect is expected to be small. Moreover, the things are somewhat balanced by the opposite effect of the adiabatic approximation that was used at the fin tips, base plate and fin edges and in the gaps between the fins at the top of the base plate.

6.2 Solution for uniform heat transfer coefficient based on fluid inlet temperature

Substituting the relation between the temperature and the heat flux distributions at the fin base, Eq. (4.9), into the heat flux continuity boundary condition, Eq. (6.4), and using the temperature continuity, Eq. (6.1), yields the boundary condition for the top of the base plate

$$-k_b \left.\frac{\partial \theta_b}{\partial y}\right|_{y=0} = \frac{k_f t}{t+b} \sum_{i=0}^{\infty} \mu_i \tanh(\mu_i l) \frac{\int_0^L \theta_b(x,0,z)\cos(\alpha_i x)\ dx}{\int_0^L \cos^2(\alpha_i x)\ dx} \cos(\alpha_i x) \qquad (6.5)$$

It is noted that although only a single fin was treated in Chapter 4, its results can be used for each value of z to obtain a boundary condition at the top of the base plate. As seen from Eq. (6.9), the boundary condition correctly describes the physics in the sense that the local heat flux at the top of the base plate is dependent on the temperatures for all the values of x, but only for the given value of z. This is because each of the fins can conduct heat in the x-direction, but there is no heat transfer between two separate fins. Naturally, the fins interact with each other through the conduction in the base plate, but this should not be seen in the boundary condition.

Substituting the general solution for the base plate temperature, Eq. (3.4), into Eq. (6.5) and using the orthogonality property of the cosine function, Eq. (A.2), gives the result

$$-k_b \sum_{i=0}^{\infty}\sum_{j=0}^{\infty} B_{ij}\cos(\alpha_i x)\cos(\beta_j z) = \frac{k_f t}{t+b}\sum_{i=0}^{\infty}\sum_{j=0}^{\infty}\mu_i \tanh(\mu_i l) A_{ij}\cos(\alpha_i x)\cos(\beta_j z) \tag{6.6}$$

The orthogonality property of the cosine function, Eq. (A.2), yields the relation between the coefficients B_{ij} and A_{ij}

$$B_{ij} = -\frac{k_f t}{t+b}\mu_i \tanh(\mu_i l) A_{ij} \tag{6.7}$$

Now, the unknown coefficients A_{ij} and B_{ij} can be solved using the boundary conditions at the bottom and top of the base plate, Eqs. (3.6) and (6.7)

$$A_{ij} = \frac{Q_{ij}}{k_b\left[\gamma_{ij}\sinh(\gamma_{ij}a) + r\mu_i \tanh(\mu_i l)\cosh(\gamma_{ij}a)\right]} \tag{6.8a}$$

$$B_{ij} = -\left[\frac{\gamma_{ij}\sinh(\gamma_{ij}a)}{r\mu_i \tanh(\mu_i l)} + \cosh(\gamma_{ij}a)\right]^{-1}\frac{Q_{ij}}{k_b} \tag{6.8b}$$

The base plate temperature distribution with the two-dimensional fin conduction taken into account can now be found by substituting Eq. (6.8) into Eq. (3.4).

Comparing Eqs. (3.12) and (6.8), it can be seen that the results obtained with the method of effective heat transfer coefficient and the method of uniform heat transfer coefficient are analogous. The only difference is that the fin parameter m in Eq. (3.12) is replaced with the parameter μ_i in Eq. (6.8) to take into account the x-direction conduction in the fins. There are many limiting cases such as $a \to \infty$ or $m \to \infty$ where the results obtained with the two methods coincide.

6.3 Solution for conjugated convection and conduction

Substituting the relation between the temperature and the heat flux distributions at the fin base, Eq. (5.20), into the heat flux continuity boundary condition, Eq. (6.4), and using the temperature continuity, Eq. (6.1), yields the boundary condition for the top of the base plate

$$-k_b \left.\frac{\partial \theta_b}{\partial y}\right|_{y=0} = \frac{k_f t}{l(t+b)}\sum_{i=0}^{N_i-1}\sum_{I=0}^{N_i-1} R_{iI}\frac{\int_0^L \theta_b(x,0,z)\cos(\alpha_I x)\ dx}{\int_0^L \cos^2(\alpha_I x)\ dx}\cos(\alpha_i x) \tag{6.9}$$

It can be seen from Eq. (6.9) that the boundary condition at the top of the base plate is an integral equation in the x-direction for each value of z, which is analogous to Eq. (6.5). Each of the fins naturally has its own temperature distribution depending on its location in the z-direction.

Substituting the general solution for the base plate, Eq. (3.4), into Eq. (6.9) and using the orthogonality property of the cosine function, Eq. (A.2), results in

$$-k_b B_{ij} = \frac{k_f t}{l(t+b)} \sum_{I=0}^{N_i-1} R_{iI} A_{Ij} \tag{6.10}$$

Substituting Eq. (6.10) into the bottom boundary condition, Eq. (3.5), yields a set of $N_i \times N_j$ linear equations for the $N_i \times N_j$ unknown coefficients A_{ij}.

$$\gamma_{ij} \sinh(\gamma_{ij} a) A_{ij} + \cosh(\gamma_{ij} a) \frac{k_f t}{k_b l(t+b)} \sum_{I=0}^{N_i-1} R_{iI} A_{Ij} = \frac{Q_{ij}}{k_b} \tag{6.11}$$

However, only N_i unknowns need to be solved simultaneously. Using the vector notation

$$\boldsymbol{a_j} = [A_{0j} \ A_{1j} \ ... \ A_{N_i-1,j}]^T \tag{6.12a}$$

$$\boldsymbol{b_j} = [B_{0j} \ B_{1j} \ ... \ B_{N_i-1,j}]^T \tag{6.12b}$$

$$\boldsymbol{q_j} = [Q_{0j} \ Q_{1j} \ ... \ Q_{N_i-1,j}]^T \tag{6.12c}$$

the solution for the unknown coefficients $\boldsymbol{a_j}$ and $\boldsymbol{b_j}$ can be written with the help of Eqs. (6.10) and (6.11) as

$$\boldsymbol{a_j} = \boldsymbol{E_j}^{-1} \frac{\boldsymbol{q_j}}{k_b} \tag{6.13a}$$

$$\boldsymbol{b_j} = -\frac{k_f t}{k_b^2 l(t+b)} \boldsymbol{R} \boldsymbol{E_j}^{-1} \boldsymbol{q_j} \tag{6.13b}$$

where $\boldsymbol{E_j} = E_{j,iI} \in \mathbb{R}^{N_i \times N_i}$ is a matrix whose diagonal elements are found by inspecting Eq. (6.11) to be

$$E_{j,ii} = \gamma_{ij} \sinh(\gamma_{ij} a) + \cosh(\gamma_{ij} a) \frac{k_f t}{k_b l(t+b)} R_{ii} \tag{6.14a}$$

while the non-diagonal elements are

$$E_{j,iI} = \cosh(\gamma_{ij} a) \frac{k_f t}{k_b l(t+b)} R_{iI} \tag{6.14b}$$

Once the coefficient vectors $\boldsymbol{a_j}$ and $\boldsymbol{b_j}$ have been calculated from Eq. (6.13) for each $j < N_j$, they can be substituted into the general base plate solution, Eq. (3.4), to obtain the temperature distribution in the whole base plate.

Chapter 7

Examples

In the preceding chapters, different solution methods have been presented for the temperature distribution at the base plate of a heat sink. The usual way of presenting heat transfer results is to form dimensionless groups and explore their relations to each other with the help of graphical presentations, tabulations and correlation equations. In the present case, however, dimensional analysis is rather ineffective.

Even for a specified pair of fluid and heat sink materials, there exist six length variables that describe the heat sink geometry. Using the Buckingham's theorem [Langhaar, p. 18], one can form five independent dimensionless groups from the length variables alone. Adding the Reynolds number, the dimensionless thermal resistance of the heat sink would depend on six dimensionless variables for each pair of materials. Moreover, the thermal resistance is naturally highly dependent on the heat source configuration at the bottom of the base plate. In principle, there are an infinite number of different heat flux distributions $q(x, z)$, depending on the number of the components, their positioning and the heat flux distributions of the individual components.

Consequently, no attempt is made here to provide any general results that could be used in a handbook way. Instead, the designer needs to implement the algorithms presented in the preceding chapters on a digital computer and perform the calculations for each heat sink design of interest. The purpose of this chapter is to illustrate the results obtained from the calculations with the help of a couple of numerical examples. Thus, the numerical values chosen in the examples are somewhat arbitrary. There was no specific reason for choosing the particular values, but the author feels that the chosen values represent realistic examples. This illustrates the differences between the calculation methods.

The geometry and the material properties used in the numerical examples are described in Section 7.1. The different calculation methods presented in the thesis are summarised in Section 7.2 for easier reference when comparing the results. Some selected results from the calculations are shown in Section 7.3 and

some discussion of the differences between the calculation methods is given in Section 7.4.

7.1 Description of examples

The dimensions of the heat sink shown in Figs. 1.1 and 1.2 were the following: $L = 0.3$ m, $H = 0.2$ m, $l = 0.1$ m, $a = 0.01$ m, $b = 0.002$ m and $t = 0.001$ m. The thermal conductivity of both the base plate and the fins was $k_b = k_f = 180$ W/mK. The properties of the fluid were taken as $k_a = 0.026$ W/mK and $\mathrm{Pr} = 0.7$, while the Reynolds number was in the laminar region, being $\mathrm{Re} = 2000$.

Two different heat source configurations were used. In the first configuration, there was a single heat source of size 0.1 m $\times$ 0.1 m located at the centre of the bottom of the base plate. The heat source generated spatially uniform heat flux of 100000 W/m^2.

In the second configuration, there were two distinct heat sources, each of size 0.1 m $\times$ 0.1 m. The first heat source generated uniform heat flux of 55000 W/m^2 and was centred at $x = 0.07$ m, $z = 0.1$ m. The second heat source generated uniform heat flux of 45000 W/m^2 and was centred at $x = 0.23$ m, $z = 0.1$ m. In both of the configurations, the total heat flux was 1000 W and the rest of the base plate was assumed insulated.

7.2 Calculation methods

The base plate temperature profiles were calculated with four different methods of different complexity, presented in the thesis. In all of the methods the Fourier coefficients Q_{ij} were calculated from Eq. (3.7) and the base plate temperature distribution from Eq. (3.4). The number of terms calculated was $N_i = N_j = 50$. Using a greater number of terms was seen to give essentially the same results.

The heat transfer coefficient h_m based on the mixed mean flow temperature was calculated from Eqs. (2.8) and (2.21). Then, the heat transfer coefficient h based on the fluid inlet temperature was calculated from Eq. (2.23). Further, the effective heat transfer coefficient h_{eff} was calculated from Eqs. (2.7) and (3.9). The values obtained were $h_m = 28.1$ W/m^{2}K, $h = 18.3$ W/m^{2}K and $h_{eff} = 464$ W/m^{2}K.

The only difference between the methods was the calculation of the coefficients A_{ij} and B_{ij} in Eq. (3.4).

1. In the method of effective heat transfer coefficient, the coefficients A_{ij} and B_{ij} were calculated from Eq. (3.12). Since this method is essentially the

method presented in [Muzychka et al. 2003], results obtained serve as a reference. The virtues and drawbacks of other methods can be assessed comparing the results to this state-of-the-art model.

2. In the method of uniform heat transfer coefficient based on the fluid inlet temperature, the coefficients A_{ij} and B_{ij} were calculated from Eq. (6.8).

3. In the method of uniform heat transfer coefficient based on the fluid mixed mean temperature, the matrix $\boldsymbol{M}^2$ was calculated from Eq. (5.11) and the matrix $\boldsymbol{R}$ was calculated from Eq. (5.19) using the eigenvalue decomposition method given in Appendix C. Finally, the coefficients A_{ij} and B_{ij} were calculated from Eqs. (6.12)–(6.14).

4. In the method of laminar hydrodynamically developed flow, the matrix $\boldsymbol{M}^2$ was calculated from Eq. (5.14) by including 30 Graetz solution eigenvalues in the summation. The matrix $\boldsymbol{R}$ was calculated from Eq. (5.19) using the eigenvalue decomposition method given in Appendix C. Finally, the coefficients A_{ij} and B_{ij} were calculated from Eqs. (6.12)–(6.14).

7.3 Results

The temperature excess distributions $\theta_b(x, -a, z)$ at the bottom of the base plate are shown in Fig. 7.1. The first and the second columns show the results for a single heat source and two distinct heat sources, respectively. The four rows show the results from the different calculation methods, in the order listed in Section 7.2.

The temperature excess profiles $\theta_b(x, -a, H/2)$ at the centreline of the bottom of the base plate obtained with different calculation methods are shown in Fig. 7.2. In the figure the four different calculation methods refer to the methods listed in Section 7.2. The two different graphs above and below correspond to the case of a single and two distinct heat sources, respectively.

To show the different treatment of the base plate top boundary condition of the different calculation methods, the effective heat transfer coefficients $h_{eff}(x, z)$ obtained with the different calculation methods and heat source configurations are plotted in Fig. 7.3. In view of Eq. (3.8), the spatially variable effective heat transfer coefficients were calculated from

$$h_{eff}(x, z) = \frac{-k_b \left.\frac{\partial \theta_b}{\partial y}\right|_{y=0}}{\theta_b(x, 0, z)} \tag{7.1}$$

The eight different plots in Fig 7.3 correspond to the same calculation methods and heat source configurations as in Fig. 7.1.

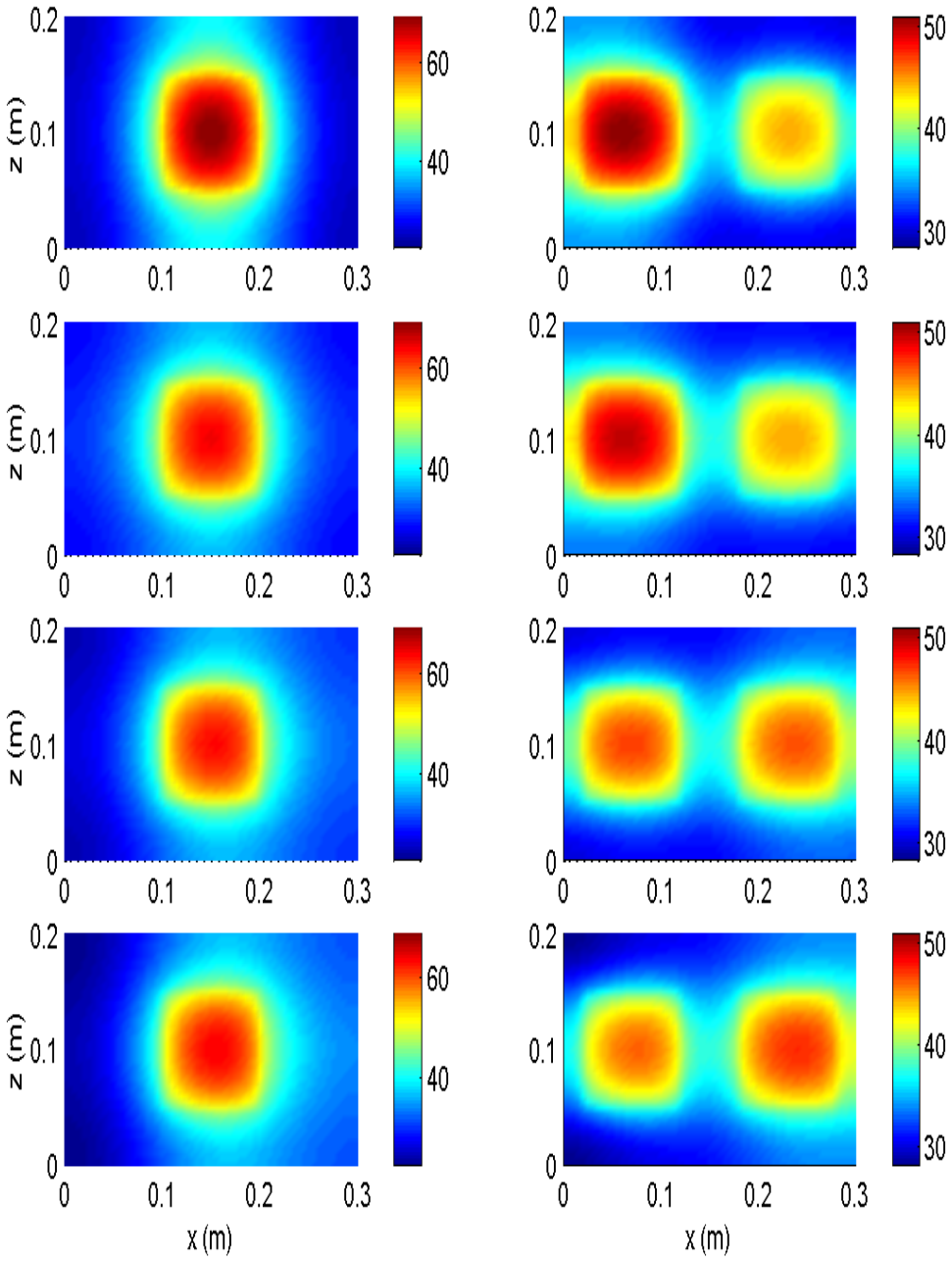

Figure 7.1: Temperature excess distributions $\theta_b(x, -a, z)$ (K) at bottom of base plate, calculated with four different methods listed in Section 7.2 and two different heat source configurations.

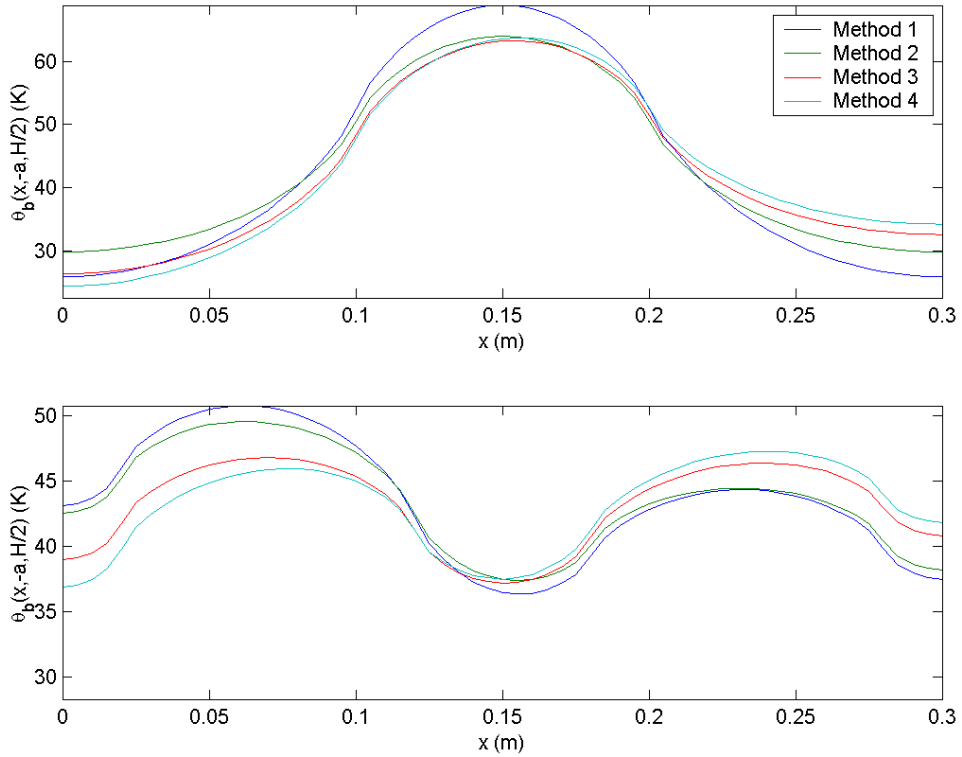

Figure 7.2: Comparison of centreline temperature excess distributions $\theta_b(x, -a, H/2)$ (K), calculated with four different calculation methods listed in Section 7.2 and two different heat source configurations.

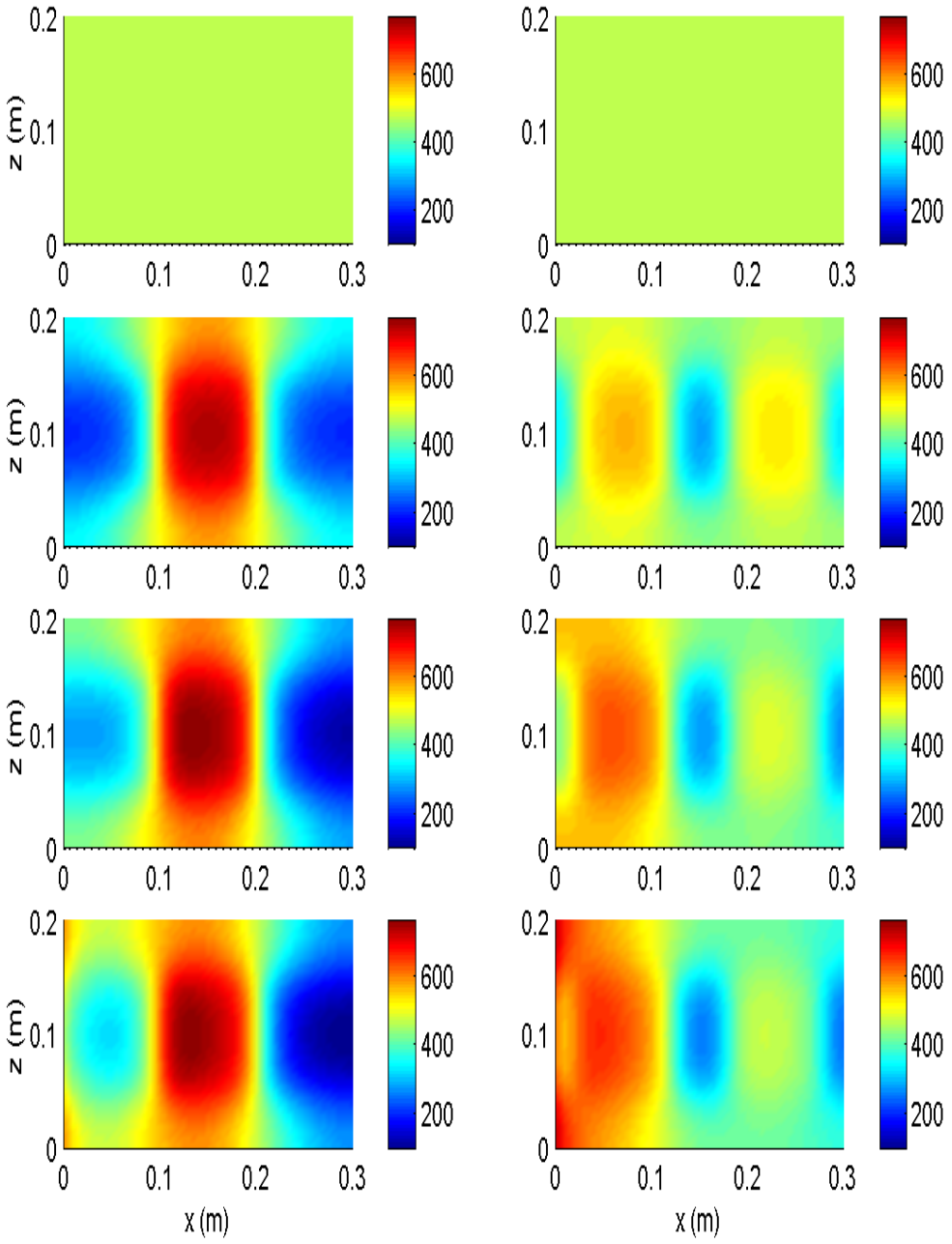

Figure 7.3: Effective heat transfer coefficients $h_{eff}(x, z)$ (W/m^{2}K) at top of base plate calculated with four different methods listed in Section 7.2 and two different heat source configurations.

7.4 Interpretations of results

For the case of a single heat source attached at the centre of the bottom of the base plate, Figs. 7.1 and 7.2 show that each of the calculation methods provide results that are qualitatively quite similar to each other. The greatest discrepancy is that the method of effective heat transfer coefficient gives significantly larger maximum temperature than the other methods.

The reason for the discrepancy is that the method of effective heat transfer coefficient does not take the x-direction conduction in the fins into account. The reason for the different results can be clearly seen from the plot of the effective heat transfer coefficients in Fig. 7.3. The methods 2–4, which take the x-direction conduction into account, have large effective heat transfer coefficients near the hot spots of the base plate. The large effective heat transfer coefficients arise from the ability of the fins to spread the heat to the colder areas. Conversely, the fins are not able to transfer much heat from the colder areas of the base plate as they are receiving remarkable amount of heat from the hotter areas of the fins through the x-direction conduction.

With the present numerical example, in which the fin mass is more that three times larger than the base plate mass, the effect of neglecting the x-direction conduction in the fins becomes significant. However, if the base plate were thicker and/or the fins were shorter and thinner, the simple method of effective heat transfer coefficient would give results much more similar to the other methods.

As can be seen from Figs. 7.1 and 7.2, the differences between the methods 2–4 listed in Section 7.2 are relatively small for the case of a single heat source. In particular, the maximum temperatures given by the three methods almost coincide. As expected, the methods 3 and 4 that take the fluid warming into account, give relatively hotter temperatures near the trailing edge of the heat sink and relatively colder temperatures near the leading edge. However, these differences between the results are of minor importance, since the maximum temperature of the components is the only thing that the designer is really interested in.

The case with two distinct heat sources gives somewhat different results. This time Figs. 7.1 and 7.2 show that the results given by the simple methods 1 and 2 differ qualitatively from the results given by the more complicated methods 3 and 4. According to the methods 1 and 2, the upstream component, which dissipates the larger amount of heat, is the hotter one. In contrast, the method 3 gives approximately equal temperatures for both of the components, while the method 4 suggests that the downstream component is the hotter one.

The reason for this discrepancy is that the first two methods do not take into account the fluid warming in the x-direction and therefore overestimate convective heat transfer near the trailing edge of the heat sink. It can be seen from Fig. 7.3 that the effective heat transfer coefficients given by the conjugated methods 3 and 4 are relatively larger near the leading edge of the heat sink.

The differences between the two methods taking the fluid warming into account are relatively small. However, the method 3, which assumes a uniform heat transfer coefficient h_m, gives slightly colder temperatures near the trailing edge of the heat sink. This is because method 4 takes into account the deterioration of the heat transfer coefficient for increasing x in laminar flows. Thus, the effective heat transfer coefficient given by the method 4 has even more skewness toward the leading edge of the heat sink than the method 3.

Chapter 8

Discussion

8.1 Recommendations

The simplest of the calculation methods presented in this thesis is the method of effective heat transfer coefficient, which can be viewed as the state-of-the-art method found in the literature. The three new calculation methods presented in this thesis each add some complexity to the calculations, while trying to describe the physics behind the problem more accurately. The question naturally is, whether the results obtained are worth the added complexity.

As discussed in Section 6.2, the results given by the first two methods actually coincide for large values of the base plate thickness a or fin parameter m. Thus, when the base plate is very thick in comparison to the fins, there is no need to include the effect of x-direction conduction in the fins.

Unfortunately, it is not easy to give any recommendation on how big the base plate thickness a and the fin parameter m need to be in order to be able to use the method of effective heat transfer coefficient, since it depends on all the other parameters in the problem. Since calculating the results from Eq. (3.12) is not significantly simpler than using Eq. (6.8), it can be recommended that the latter is always preferred to the former. However, one needs to bear in mind that both of the results were derived using several approximations which may cause errors larger than the differences between the two models.

The methods 3 and 4, as listed in Section 7.2, take the treatment of the problem to the next level. Much more physics is introduced to the solution by allowing the convective heat flux from the fins to respond to the changes in the fluid mixed mean temperature or the whole upstream fin temperature distribution. It is no longer possible to obtain a fully analytical solution in these conjugated heat transfer cases.

However, the solutions can be very easily and rapidly computed using standard linear algebra procedures such as eigenvalue decomposition and Gaussian elim-

ination. Moreover, the matrices $\boldsymbol{R}$ and $\boldsymbol{E_j}$ need to be calculated only once for each geometry and mass flow rate. This makes the optimisation of the heat source placement very efficient, since only the coefficients Q_{ij} need to be recalculated, after which the result in Eq. (6.13) can be directly used.

In the cases of a single heat source, it is quite safe to ignore the effect of fluid warming and use Eq. (6.8). This is especially true if the single heat source is attached near the centre of the bottom of the base plate. In contrast, when there are two or more heat sources placed such that one heat source is located in the wake of another, it is usually preferable to use the conjugated solution in Eq. (6.13).

However, the simpler Eq. (6.8) may give feasible results in some cases even with several heat sources. One such an example is a nearly isothermal base plate, when the total amount of convective heat transfer becomes much more important than its spatial distribution. Another example would be a very high mass flow rate ($N_{tu} \leq 0.1$) which results in only slightly warming mixed mean flow temperature.

For laminar flows, the differences between the conjugated methods 3 and 4 as listed in Section 7.2 are usually quite small. An important advantage of the method 3 over the method 4 is that it can be used for both laminar and turbulent flows, as long as the correct convection formulae in Sections 2.2–2.3 are used. In contrast, the method 4 is only applicable for laminar flows.

It is a difficult choice between the methods 3 and 4 in the laminar case. The computational effort is of the same order of magnitude in both of the methods, being slightly higher for the method 4. The method 3, which assumes a uniform heat transfer coefficient based on the mixed mean flow temperature, tends to underestimate heat transfer near the leading edge of the heat sink and overestimate the heat transfer near the trailing edge of the heat sink. On the other hand, the method 4, which assumes a hydrodynamically fully developed flow, tends to underestimate the overall heat transfer, especially for air-cooled heat sinks that are very short.

For liquid-cooled laminar-flow heat sinks, the method 4 is always the more accurate, as the Graetz solution can be viewed as exact. For air-cooled heat sinks, the choice is more difficult. The longer the heat sink is, the better the method 4 performs. As a rule of thumb, the method 4 is to be preferred when $L^+ > 0.02$. However, the method 3 may be the more accurate far beyond that limit if the heat sink is very isothermal. Luckily, as said above, the differences between the methods 3 and 4 are quite small in most engineering calculations.

8.2 Limitations and possible generalisations of calculation methods

There are several physical phenomena that all the calculation methods presented in the thesis fail to describe. First of all, the thermal radiation was neglected. This is not usually a big issue in forced convection since the convection is the dominating mode of heat transfer.

Furthermore, the heat was assumed to leave the base plate only through the fins. Usually the fin heat transfer area is very large when compared to the base plate area, which justifies this assumption. The same applies to the adiabatic approximation at the tips and edges of the fin.

Moreover, the junction was treated in an approximate way neglecting the contact and constriction resistances. The effect of a contact resistance that depends linearly on the local heat flux may be incorporated into the boundary condition in Eq. (6.4) quite easily. The contact resistance was neglected in the present treatment in order to keep the equations as simple as possible.

In contrast, the effect of the constriction resistance at the junction between the base plate and the fins is somewhat more difficult to include in the present formulation. If this effect is significant, some correction factors will probably have to be used. Luckily, the effect of the constriction resistance is significant only for very thin base plates and large fin spacings. The effect of the three-dimensional fin temperature has also been neglected. The effect of non-uniform fin temperature in the z-direction is negligible as long as the transverse Biot number is much less than unity, $\frac{ht}{k_f} \ll 1$ [Ma et al.].

For simplicity, isotropic heat conductivity was assumed throughout the thesis. The whole analysis can be equally well done for base plates and fins having different heat conductivities in the x-, y- and z-directions. The purpose of assuming isotropy was again to keep the equations relatively simple.

Finally, the methods presented in the thesis can be extended to the transient operation of the heat sink in a straightforward way. This would be done by Laplace transforming the time-dependent heat equation for both the base plate and the fins. Then, the analysis would be carried out in the Laplace domain in the way described in the thesis. This would correspond to treating the convection with the quasi-static approximation, which is very accurate due to the great heat capacity of the solids [Arpaci & Larsen, p. 181]. Finally, the desired transient base plate temperature would be obtained using a numerical inverse Laplace transform algorithm.

8.3 Other methods of solution

The natural alternative for the methods presented in the thesis is to use computational fluid dynamics to determine the temperature field. This is a perfectly valid approach, but the computational effort would be much higher than that of the present methods. Much effort would be needed to solve the momentum and energy equations in the fluid but the accuracy of the results is expected to be virtually the same as that of the present methods 3 and 4. Moreover, great attention would be needed to ensure convergence when computing conjugated conduction and convection heat transfer.

Another alternative would be to calculate the base plate and the fins with a standard numerical partial differential equation solution method, such as the finite difference method, the finite volume method or the finite element method. The convection would be coupled to the solution using the same formulae as in the thesis, namely Eqs. (2.14) or (5.3). The computational effort involved in this approach is significantly smaller than that of the computational fluid dynamics method, but still greater than that of the methods presented in the thesis.

In the finite difference method, for example, the solution method would probably be iterative. If a non-iterative solution is desired, one needs to solve temperatures of all the nodes in the heat sink simultaneously. This corresponds to inverting a sparse matrix, which is a fairly frequent task in numerical linear algebra. In the present case, however, the things are quite complicated as the bandwidth of the matrix is relatively large. This is because the energy balance at the trailing edge of the fin is affected by the whole upstream fin temperature distribution, as can be seen from the integral in Eqs. (2.14) or (5.3).

Chapter 9

Conclusions

In this thesis, new calculation methods have been developed for rectangular plate-fin heat sinks cooled by forced convection. The traditional fin theory has been extended by allowing the fin temperature to vary in the direction of the flow and allowing the convective heat flux from the fins to be modelled more accurately than just using a uniform heat transfer coefficient h. The methods can be used for any prescribed heat source configuration at the bottom of the base plate.

Using an approximate treatment of the junction between the base plate and the fins, three new solution methods were presented with which one can solve the base plate temperature using the newly developed solutions for the fin temperature. With a realistic numerical example, it was shown that the new methods may give results that significantly differ from the state-of-the-art method of effective heat transfer coefficient.

It was shown that the method of effective heat transfer coefficient is a special case of the new methods. Since the new methods include more physics, it is expected that they can perform no worse than the method of effective heat transfer. However, the improvement in the accuracy comes at the cost of some complexity.

In the method of uniform heat transfer coefficient based on inlet temperature, the added complexity is very small. The computational effort is very small, being virtually the same as in the method of effective heat transfer coefficient. In contrast, the conjugated methods which take the warming of the fluid into account are somewhat more complicated to use. The solution procedure involves computing a matrix function and solving several sets of linear equations. However, the solution is very efficient with the standard numerical mathematics software. The computing times are typically in the order of seconds. This makes the present methods preferable to computational fluid dynamics in many cases.

The suitability of the calculation methods for different cases was also discussed. The method of uniform heat transfer coefficient based on mixed mean temperature was recommended to be used in most engineering calculations with turbulent flows. For laminar flows, the method of hydrodynamically fully developed flow

is preferable for liquid-cooled or very long air-cooled heat sinks. However, for a single heat source or for a high mass flow rate, the simple method of uniform heat transfer coefficient based on fluid inlet temperature gives good results.

Finally, generalising the methods presented in the thesis for the transient operation of the heat sink was shortly discussed. This leads to an efficient algorithm for a bottom heat flux which varies arbitrarily both spatially and temporally.

Appendix A

Fourier cosine series

Any function $f(x)$ can be expressed as the Fourier cosine series in the interval $0 < x < L$ [Strauss, p. 103]

$$f(x) = \sum_{i=0}^{\infty} f_i \cos\left(\frac{i\pi x}{L}\right) \tag{A.1}$$

Note that most textbooks use the convention that f_0 is divided by 2 in the series in Eq. (A.1). The advantage of this definition is that the norms of each of the basis functions are equal. For the purposes of this thesis, however, the above definition for the Fourier cosine series is more convenient.

The cosine function has the orthogonality property

$$\int_0^L \cos\left(\frac{i\pi x}{L}\right) \cos\left(\frac{I\pi x}{L}\right)\, dx = 0 \quad \text{if } i \neq I \tag{A.2}$$

The integral over the cosine function squared is also frequently needed

$$\int_0^L \cos^2\left(\frac{i\pi x}{L}\right)\, dx = \frac{2L}{1+\delta(i)} \tag{A.3}$$

where

$$\delta(i) = \begin{cases} 1 & \text{for } i = 0 \\ 0 & \text{for } i \neq 0 \end{cases} \tag{A.4}$$

Using Eqs. (A.1)–(A.3) the Fourier coefficients f_i can be solved as

$$f_i = \frac{1+\delta(i)}{2L}\int_0^L f(x)\cos\left(\frac{i\pi x}{L}\right)\,dx \tag{A.5}$$

The Fourier cosine series in the right hand side of Eq. (A.1) converges uniformly to $f(x)$ on $0 \le x \le L$ provided that [Strauss, p. 124]

1. $f(x)$, $f'(x)$, and $f''(x)$ exist and are continuous for $0 \le x \le L$ and
2. $f(x)$ satisfies the given boundary conditions

The uniform convergence is very important since it allows term-by-term differentiation of the series. All the Fourier cosine series occurring in the thesis are uniformly convergent. The derivatives of the temperature exist and are continuous due to the nature of heat conduction and absence of heat sources inside the base plate or the fins. Also the second condition above is satisfied, since the cosine series fit to the adiabatic boundary conditions at the edges of the base plate and the fins.

Functions of several variables can also be expressed in the form of Fourier cosine series [Strauss, pp. 140, 155–158]. For example, the function $f(x,y)$ can be expanded in $0 < x < L,\ 0 < y < l$

$$f(x,y) = \sum_{i=0}^{\infty} f_i(y)\cos\left(\frac{i\pi x}{L}\right) \tag{A.6}$$

or the function $f(x,y,z)$ can be expanded in $0 < x < L, 0 < y < l, 0 < z < H$

$$f(x,y,z) = \sum_{i=0}^{\infty}\sum_{j=0}^{\infty} f_{ij}(y)\cos\left(\frac{i\pi x}{L}\right)\cos\left(\frac{j\pi z}{H}\right) \tag{A.7}$$

Appendix B

Some integrals

Some integrals occurring in the thesis are presented in this appendix to improve readability of the text.

$$\begin{aligned}
&\int_0^x \exp\left[N_{tu}\left(\frac{\xi - x}{L}\right)\right]\cos(\alpha_I \xi)\ d\xi \\
&= e^{-N_{tu}\frac{x}{L}} \int_0^x e^{-N_{tu}\frac{\xi}{L}} \cos\left(\frac{I\pi\xi}{L}\right)\ d\xi \\
&= e^{-N_{tu}\frac{x}{L}} \Big/_{\xi=0}^{x} \frac{Le^{-N_{tu}\frac{\xi}{L}}\left[N_{tu}\cos\left(\frac{I\pi\xi}{L}\right) + I\pi\sin\left(\frac{I\pi\xi}{L}\right)\right]}{N_{tu}^2 + (I\pi)^2} \\
&= \frac{N_{tu}L\left[\cos(\alpha_I x) - e^{-N_{tu}\frac{x}{L}}\right] + I\pi L\sin(\alpha_I x)}{N_{tu}^2 + (I\pi)^2}
\end{aligned} \tag{B.1}$$

$$\begin{aligned}
&\int_0^L e^{-N_{tu}\frac{x}{L}}\cos(\alpha_i x)\ dx \\
&= \int_0^L e^{-N_{tu}\frac{x}{L}}\cos\left(\frac{i\pi x}{L}\right)\ dx \\
&= \Big/_{x=0}^{L} \frac{Le^{-N_{tu}\frac{x}{L}}\left[i\pi\sin\left(\frac{i\pi x}{L}\right) - N_{tu}\cos\left(\frac{i\pi x}{L}\right)\right]}{N_{tu}^2 + (i\pi)^2} \\
&= -\frac{LN_{tu}\left[e^{-N_{tu}}\cos(i\pi) - 1\right]}{N_{tu}^2 + (i\pi)^2} \\
&= \frac{LN_{tu}\left[1 - (-1)^i e^{-N_{tu}}\right]}{N_{tu}^2 + (i\pi)^2}
\end{aligned} \tag{B.2}$$

$$\begin{aligned}
&\int_0^L \sin(\alpha_i x)\cos(\alpha_i x)\ dx \\
&= \frac{1}{2}\int_0^L \sin\left(\frac{2i\pi x}{L}\right)\ dx = 0
\end{aligned} \tag{B.3a}$$

$$
\begin{aligned}
&\int_0^L \sin(\alpha_I x)\cos(\alpha_i x)\ dx \\
&= \int_0^L \sin\left(\frac{I\pi x}{L}\right)\cos\left(\frac{i\pi x}{L}\right)\ dx \\
&= \frac{1}{2}\int_0^L \left[\sin\left(\frac{(I+i)\pi x}{L}\right) + \sin\left(\frac{(I-i)\pi x}{L}\right)\right]\ dx \\
&= -\frac{1}{2}\Big/_{x=0}^{L}\left[\frac{L}{(I+i)\pi}\cos\left(\frac{(I+i)\pi x}{L}\right) + \frac{L}{(I-i)\pi}\cos\left(\frac{(I-i)\pi x}{L}\right)\right] \\
&= -\frac{1}{2}\left[\frac{L}{(I+i)\pi}\left((-1)^{i+I}-1\right) + \frac{L}{(I-i)\pi}\left((-1)^{I-i}-1\right)\right] \\
&= -\frac{1}{2}\left[\frac{L}{(I+i)\pi}\left((-1)^{i+I}-1\right) + \frac{L}{(I-i)\pi}\left((-1)^{I+i}-1\right)\right] \\
&= \frac{LI\left(1-(-1)^{I+i}\right)}{\pi(I^2-i^2)}
\end{aligned}
\tag{B.3b}
$$

$$
\begin{aligned}
&\int_{\xi=0}^{x^+} e^{-\lambda_n^2(x^+-\xi)}\frac{d\cos\left(\frac{\alpha_I x}{x^+}\xi\right)}{d\xi}\ d\xi \\
&= -\left(\frac{\alpha_I x}{x^+}\right)e^{-\lambda_n^2 x^+}\int_{\xi=0}^{x^+} e^{\lambda_n^2\xi}\sin\left(\frac{\alpha_I x}{x^+}\xi\right)\ d\xi \\
&= \left(\frac{\alpha_I x}{x^+}\right)e^{-\lambda_n^2 x^+}\Big/_{\xi=0}^{x^+}\frac{e^{\lambda_n^2\xi}\left[\left(\frac{\alpha_I x}{x^+}\right)\cos\left(\frac{\alpha_I x\xi}{x^+}\right) - \lambda_n^2\sin\left(\frac{\alpha_I x\xi}{x^+}\right)\right]}{\lambda_n^4 + \left(\frac{\alpha_I x}{x^+}\right)^2} \\
&= \frac{\left(\frac{\alpha_I x}{x^+}\right)^2\left[\cos(\alpha_I x) - e^{-\lambda_n^2 x^+}\right] - \lambda_n^2\left(\frac{\alpha_I x}{x^+}\right)\sin(\alpha_I x)}{\lambda_n^4 + \left(\frac{\alpha_I x}{x^+}\right)^2} \\
&= \frac{(I\pi)^2\left[\cos(\alpha_I x) - e^{-\lambda_n^2 x^+}\right] - \lambda_n^2 L^+ I\pi\sin(\alpha_I x)}{\left(\lambda_n^2 L^+\right)^2 + (I\pi)^2}
\end{aligned}
\tag{B.4}
$$

Analogously to Eq. (B.2):

$$
\begin{aligned}
&\int_0^L e^{-\lambda_n^2 x^+}\cos(\alpha_i x)\ dx \\
&= \int_0^L e^{-\frac{\lambda_n^2 L^+}{L}x}\cos\left(\frac{i\pi x}{L}\right)\ dx \\
&= \frac{L\lambda_n^2 L^+\left(1-(-1)^i e^{-\lambda_n^2 L^+}\right)}{\left(\lambda_n^2 L^+\right)^2 + (i\pi)^2}
\end{aligned}
\tag{B.5}
$$

Appendix C

Matrix functions

The matrix exponential can be defined as [Golub & Van Loan, p. 540]

$$e^{\boldsymbol{X}} = \sum_{p=0}^{\infty} \frac{\boldsymbol{X}^p}{p!} \tag{C.1}$$

Direct differentiation of Eq. (C.1) shows that

$$\frac{de^{\boldsymbol{X}y}}{dy} = \boldsymbol{X}e^{\boldsymbol{X}y} = e^{\boldsymbol{X}y}\boldsymbol{X} \tag{C.2}$$

Analogously to the scalar case, one can define the hyperbolic matrix functions

$$\cosh(\boldsymbol{X}) = \frac{e^{\boldsymbol{X}} + e^{-\boldsymbol{X}}}{2} \tag{C.3}$$

$$\sinh(\boldsymbol{X}) = \frac{e^{\boldsymbol{X}} - e^{-\boldsymbol{X}}}{2} \tag{C.4}$$

$$\tanh(\boldsymbol{X}) = \left(e^{\boldsymbol{X}} + e^{-\boldsymbol{X}}\right)^{-1}\left(e^{\boldsymbol{X}} - e^{-\boldsymbol{X}}\right) \tag{C.5}$$

Using Eqs. (C.2)–(C.4) shows that

$$\frac{d\cosh(\boldsymbol{X}y)}{dy} = \boldsymbol{X}\sinh(\boldsymbol{X}y) = \sinh(\boldsymbol{X}y)\boldsymbol{X} \tag{C.6}$$

and

$$\frac{d\sinh(\boldsymbol{X}y)}{dy} = \boldsymbol{X}\cosh(\boldsymbol{X}y) = \cosh(\boldsymbol{X}y)\boldsymbol{X} \tag{C.7}$$

One approach to compute matrix functions such as the matrix $\boldsymbol{R}$ in Eq. (5.19) is to compute an eigenvalue decomposition

$$\boldsymbol{M}^2 = \boldsymbol{V}\boldsymbol{\Lambda}^2\boldsymbol{V}^{-1} \tag{C.8}$$

where $\boldsymbol{\Lambda}^2$ is a diagonal matrix composed of the eigenvalues of the matrix $\boldsymbol{M}^2$ while $\boldsymbol{V}$ is a matrix composed of the eigenvectors of the matrix $\boldsymbol{M}^2$. The eigenvalue decomposition can be routinely computed with numerical mathematics software such as Matlab. It can easily be seen that one of the square roots of the matrix $\boldsymbol{M}^2$ is given by

$$\boldsymbol{M} = \boldsymbol{V}\boldsymbol{\Lambda}\boldsymbol{V}^{-1} \tag{C.9}$$

where the diagonal matrix $\boldsymbol{\Lambda}$ is obtained by simply taking the element-wise square root of the diagonal matrix $\boldsymbol{\Lambda}^2$. The virtue of the eigenvalue decomposition is that all the matrix functions can be computed by calculating the function values of the eigenvalues of the original matrix [Golub & Van Loan, p. 539]

$$f(\boldsymbol{M}) = \boldsymbol{V}f(\boldsymbol{\Lambda})\boldsymbol{V}^{-1} \tag{C.10}$$

Therefore, the matrix $\boldsymbol{R}$ in Eq. (5.19) takes the following form

$$\boldsymbol{R} = \boldsymbol{M}l\tanh(\boldsymbol{M}l) = \boldsymbol{V}\boldsymbol{\Lambda}l\tanh(\boldsymbol{\Lambda}l)\boldsymbol{V}^{-1} \tag{C.11}$$

where $\tanh(\boldsymbol{\Lambda}l)$ is a diagonal matrix resulting from taking an element-wise hyperbolic tangent of the diagonal elements of the matrix $\boldsymbol{\Lambda}l$.

In general, the method of eigenfunction decomposition may lead to numerical instability as the errors in evaluating $f(\boldsymbol{\Lambda})$ can be magnified by as much as $\|\boldsymbol{V}\|\|\boldsymbol{V}^{-1}\|$. These problems can be avoided by using more advanced decomposition methods, such as the Schur-Parlett algorithm presented in [Davies & Higham].

However, the eigenvalue decomposition method is expected to perform sufficiently well for the matrix $\boldsymbol{M}^2$. This is because the matrix $\boldsymbol{M}^2$ is very diagonally-dominant, as can be seen by inspecting Eqs. (5.11) and (5.14). Physically, this results from the large stabilising effect of the x-direction conduction in the fins.

Bibliography

[Arpaci & Larsen] Arpaci, Vedat S. & Larsen, Poul S. *Convection Heat Transfer*. Prentice-Hall, Inc., 1984. 512 p.

[Bejan & Morega] Bejan, A. & Morega, Al. M. "*The optimal spacing of a stack of plates cooled by turbulent forced convection*", Int. J. Heat Mass Transfer, vol. 37(6), 1994. pp. 1045–1048

[Bejan & Sciubba] Bejan, Adrian & Sciubba, Enrico. "*The optimal spacing of parallel plates cooled by forced convection*", Int. J. Heat Mass Transfer, vol. 35(12), 1992. pp. 3259–3264

[Buikis et al.] Buikis, A., Buike, M. & Guseinov, S. "*Analytical two-dimensional solutions for heat transfer in a system with rectangular fin*" in B. Sundén et. al. (Eds.): Advanced Computational Methods in Heat Transfer VIII, WITPress, Southampton, 2004. pp. 35–46.

[Culham & Yovanovich] Culham, J.R. & Yovanovich, M.M. "*Non-Iterative Technique for Computing Temperature Distributions in Flat Plates with Distributed Sources and Convective Cooling*", Second ASME–JSME Thermal Engineering Joint Conference, Honolulu, Hawaii, 1987. pp. 403–409.

[Culham et al.] Culham, J.R., Teertstra, P. & Yovanovich, M.M. "*Thermal Wake Effects in Printed Circuit Boards*", Journal of Electronics Manufacturing, vol. 9(2), 2000. pp. 99–106.

[Davies & Higham] Davies, Philip I. & Higham, Nicholas J. "*A Schur-Parlett Algorithm for Computing Matrix Functions*", Siam J. Matrix Anal. Appl. 25(2), 2003. pp. 464–485.

[Golub & Van Loan] Golub, Gene H. & Van Loan, Charles F. *Matrix Computations*, 2nd ed. The John Hopkins University Press, 1989. 642 p.

[Hewitt] Hewitt, Geoffrey F. *Heat Exchanger Design Handbook*. Begell House, Inc., 1998. 3340 p.

[Incropera] Incropera, Frank P. *Liquid Cooling of Electronic Devices by Single Phase Convection*. John Wiley & Sons, Inc., 1999. 285 p.

[Incropera & DeWitt] Incropera, Frank P. & DeWitt, David P. *Fundamentals of heat and mass transfer*, 3rd ed. John Wiley & Sons, 1990. 919 p.

[Karvinen et al.] Karvinen, R., Lehtinen, A., Aittomäki, A. "*Efficiency of Dry-Wet Fin in Air COnditioning*", Proceedings of th Baltic Heat Transfer Conference, 2003. pp. 671–678.

[Karvinen] Karvinen, R. "*Natural and forced convection heat transfer from a plate fin*", Int. J. Heat Mass Transfer, vol. 24 (5), 1981. pp. 881-885.

[Kays et al.] Kays, W.M., Crawford, M.E. & Weigand Bernhard. *Convective Heat and Mass Transfer*, 4th ed. McGraw-Hill, 2005. 546 p.

[Khan et al.] Khan, W., Culham, J.R. & Yovanovich, M.M. "*The Role of Fin Geometry in Heat Sink Performance*", International Electronic Packaging Technical Conference and Exhibit, 2003.

[Kraus] Kraus, Allan D. *Analysis and evaluation of extended surface thermal systems*. Hemisphere Publishing Corporation, 1982. 560 p.

[Langhaar] Langhaar, Henry L. *Dimensional Analysis and Theory of Models*. John Wiley & Sons, Inc, 1951. 166 p.

[Lee et al.] Lee, S., Song, S., Au, V. & Moran, K.P. "*Constriction/Spreading Resistance Model for Electronic Packaging*", Proceedings of ASME/JSME Engineering Conference, vol. 4, 1995.

[Lehtinen & Karvinen 2004] Lehtinen, A. & Karvinen, R. "*Analytical Three-Dimensional Solution for Heat Sink Temperature*", Proceedings of IMECE2004, 2004.

[Lehtinen & Karvinen 2005] Lehtinen, A. & Karvinen, R. "*Conjugated heat transfer in a package of fins*" in C.A. Brebbia & G.M. Carlomagno (Eds.): Computational Methods and Experimental Measurements XII, WITPress, Southampton, 2005. pp. 737–746.

[Ma et al.] Ma, S.W., Behbahani, A.I. & Tsuei, Y.G. "*Two-dimensional rectangular fin with variable heat transfer coefficient*", Int. J. Heat Mass Transfer, vol. 34(1), 1991. pp. 79–85.

[Mereu et al.] Mereu, S., Sciubba, E. & Bejan, A. "*The optimal cooling of a stack of heat generating boards with fixed pressure drop, flowrate or pumping power*", Int. J. Heat Mass Transfer, vol. 36(15), 1993. pp. 3677–3686.

[Muzychka et al. 2003] Muzychka, Y.S., Culham, J.R., Yovanovich, M.M. "*Thermal Spreading Resistance of Eccentric Heat Sources on Rectangular Flux Channels*", Journal of Electronic Packaging, vol. 125, 2003. pp. 178–185.

[Muzychka et al. 2004] Muzychka, Y.S., Yovanovich, M.M. & Culham, J.R. "*Applications of Thermal Spreading Resistance in Compound and Orthotropic Systems*", AIAA Journal of Thermophysics and Heat Transfer, vol. 18, 2004. pp. 45–51.

[da Silva et al.] da Silva, A. K., Lorente, S. & Bejan, A. "*Optimal distribution of discrete heat sources on a plate with laminar forced convection*", Int. J. Heat Mass Transfer, vol. 47(10–11), 2004. pp. 2139-2148.

[Shah & London] Shah, R.K. & London, A.L. *Laminar Flow Forced Convection in Ducts*. Academic Press, 1978. 477 p.

[Spanier & Oldham] Spanier, J. & Oldham, K.B. *An Atlas of Functions*, Hemisphere Publishing Corporation, 1987. 700 p.

[Sparrow & Lee] Sparrow, E.M. & Lee, L. "*Effects of Fin Base-Temperature Depression in a Multifin Array*", ASME Journal of Heat Transfer, vol. 97(3), 1975. pp. 463–465.

[Strauss] Strauss, Walter A. *Partial differential equations: An introduction*. John Wiley & Sons, Inc., 1992. 425 p.

[Teertstra et al.] Teertstra, P., Yovanovich, M.M. & Culham, J.R. "*Analytical Forced Convection Modeling of Plate Fin Heat Sinks*", Journal of Electronics Manufacturing, vol. 10 (4), 2000. pp. 253–261.

[Ünal] Ünal, H.C. "*Determination of the temperature distribution in an extended surface with a non-uniform heat transfer coefficient*", Int. J. Heat Mass Transfer, vol. 28, 1985. pp. 2279–2284.

[Yeh & Chang] Yeh, Rong-Hua & Chang, Ning. "*Optimum Longitudinal Convective Fin Arrays*", International Communications in Heat and Mass Transfer, vol. 22(3), 1995. pp. 445-460.

[Yovanovich et al.] Yovanovich, M.M., Muzychka, Y.S., Culham, J.R, "*Spreading Resistance of Isoflux Rectangles and Strips on Compound Flux Channels*", AIAA Journal of Thermophysics and Heat Transfer 13 (4), 1999. pp. 494–500.

Tampereen teknillinen yliopisto
PL 527
33101 Tampere

Tampere University of Technology
P.O. Box 527
FIN-33101 Tampere, Finland